Syntheses, Carbonylations, and Dihydrogen Exchange Studies of Monomeric and Dimeric Silox ($^tBu_3SiO^-$) Hydrides of Tantalum: Structure of $[(silox)_2TaH_2]_2$

Rebecca L. Miller, Robert Toreki, Robert E. LaPointe, Peter T. Wolczanski,* Gregory D. Van Duyne, and D. Christopher Roe†

Contribution from the Department of Chemistry, Baker Laboratory, Cornell University, Ithaca, New York 14853

Received September 21, 1992

Abstract: Reduction of $(silox)_3TaCl_2$ (**1**) (silox = $^tBu_3SiO^-$) with Na/Hg in THF under H_2 afforded $(silox)_3TaH_2$ (**2**, 43%); **2** thermally cyclometalated to $(silox)_2HTaOSi^tBu_2CMe_2CH_2$ (**4**), but was reconstituted with H_2 (6 days, 3 atm). Treatment of **2** with C_2H_4, neat CCl_4, and CH_3I in Et_2O generated $(silox)_3HTaEt$ (**5**, 63%), $(silox)_3HTaCl$ (**6**-Cl, 63%), and $(silox)_3HTaI$ (**6**-I, 62%). Reduction of $(silox)_3HTaI$ (**6**-I) with Na/Hg in THF produced a ring-opened THF compound, $[(silox)_3TaH]_2(\mu{:}\eta^1,\eta^1\text{-}CH_2(CH_2)_3O)$ (**7**, 58%). Photolysis of $(silox)_2Cl_2TaCH_2Ph$ (**8**) under 3 atm of H_2 gave $[(silox)_2TaCl)]_2(\mu\text{-}H)_2$ (**10**), C_7H_8, and a trace of bibenzyl. Reduction of $(silox)_2TaCl_3$ (**9**) with Na/Hg under 1 atm of H_2 (~15 days) yielded an unbridged D_{2d} dimer $[(silox)_2TaH_2]_2$ (**11**, 83%), which possessed a 2.720(4) Å Ta–Ta bond. Crystal data for **11**: cubic, $I\bar{4}3d$, a = 28.125(6) Å, Z = 12, T = 23 °C, 1190 reflections ($F > 3.0\sigma(F)$), R = 0.079, and R_w = 0.050. Exposure of **11** to 2 equiv of HCl, 1.0 equiv of O_2, and 1.0 equiv of Me_3NO provided **10** (78%), $[(silox)_2TaH]_2(\mu\text{-}O)_2$ (**12**, 95%), and $[(silox)_2TaH]_2(\mu\text{-}H)_2(\mu\text{-}O)$ (**14**, 67%); derivatization of **12** with C_2H_4 gave $[(silox)_2TaCH_2CH_3]_2(\mu\text{-}O)_2$ (**13**, 39%). μ-Oxo dimer **14** exists as two C_2 isomers; the hydrides of **14a** exchanged with $\Delta G^\ddagger \approx 8$ kcal/mol, while those of **14b** exchanged coincidently with interconversion of the isomers ($\Delta G^\ddagger \approx 11$ kcal/mol; **14a** ⇌ **14b**, ΔH = –1.1(3) kcal/mol, ΔS = –4.6(9) eu). Isotopomers $(silox)_4Ta_2D_nH_{4-n}$ (**11**-d_n) were distinguished by a +0.022 ppm/D (23 °C) NMR isotope shift. Dihydride **2** undergoes σ-bond metathesis with D_2, initially forming $(silox)_3TaHD$ (**2**-d_1), and the exchange of **11** with H_2 was directly measured by spin saturation transfer ^1H NMR techniques (50 °C, k = 9.2(3) × 10^2 M^{-1} s^{-1}; $\Delta H^\ddagger$ = 6.2(1) kcal/mol, $\Delta S^\ddagger$ = –26(3) eu). Carbonylation of **2** and **5** afforded η^2-aldehydes $(silox)_3Ta(\eta^2\text{-}OCHR)$ (R = H, **15**, 77%; Et, **16**, 41%), alternatively prepared from $(silox)_3Ta$ (**3**) and CH_2O and EtCHO, respectively. Only **15** and **15**-d_2 were generated from **2** and **2**-d_2 (5 atm). Spectroscopic, ^{13}C-labeling, and protic quenching studies confirmed the constitutions of various dimeric carbonylation products. Treatment of **10** with CO yielded $[(silox)_2TaCl]_2(\mu\text{-}H)(\mu{:}\eta^2,\eta^2\text{-}CHO)$ (**18**, 56%), while exposure of **11** to ~1.0 equiv of CO afforded $[(silox)_2TaH]_2(\mu\text{-}CH_2)(\mu\text{-}O)$ (**19**, 67%). Reformation of the C–O bond occurred when **19** was carbonylated. $[(silox)_2TaH](\mu{:}\eta^2,\eta^2\text{-}CHO)(\mu{:}\eta^1,\eta^2\text{-}CH_2O)[Ta(silox)_2]$ (**20**) was isolated in 55% yield and converted (1 h, 60 °C) to $[(silox)_2Ta]_2(\mu\text{-}O)_2(\mu\text{-}CHMe)$ (**21**, 61%). The sequence **11** + CO → **19** → **20** → **21** exhibits the critical C–O bond-breaking and the C–H and C–C bond-making events of the Fischer–Tropsch (F-T) process. Extended exposure of **11** or **20** to 1 atm of CO provided $[(silox)_2Ta]_2(\mu{:}\eta^1,\eta^1\text{-}CH{=}CHO)(\mu{:}\eta^1,\eta^2\text{-}CH_2O)(\mu\text{-}O)$ (**22**, 50%). Carbonylation of **12** generated $[(silox)_2Ta]_2(\mu\text{-}O)_2(\mu\text{-}CH_2O)$ (**23**) as the major product (70–90%), while treatment of **14** with CO yielded first $[(silox)_2HTa](\mu\text{-}O)_2[TaMe(silox)_2]$ (**24**, 90%) and then $[(silox)_2Ta]_2(\mu\text{-}O)_2(\mu\text{-}MeCHO)$ (**25**, ~90%). ^{13}CO-labeling studies were used to follow the **19** → **21** and **22** conversions, providing the basis of a mechanistic assessment. Dimeric structures allow oxygenated fragments to remain coordinated to two tantalums throughout the sequence. Insertion into Ta–H bonds may initiate each carbonylation process. Stereochemical consequences of silox ligation are discussed in relation to the structures and dynamics of the binuclears, while the electrophilic tantalum centers are important in H/D exchange and carbonylation chemistry. The carbonylation chemistry underscores three critical points regarding the F-T process: (1) hydride transfer to CO is a reasonable alternative to CO dissociation; (2) adsorbed hydrocarbyl and oxygenate fragments are related by reversible C–O bond-breaking and bond-making events; and (3) oxygenate and hydrocarbyl adsorbates can be removed protolytically, akin to hydrogenation.

Introduction

The Fischer–Tropsch (F-T) process,[1,2] while not a panacea for future energy needs, remains a viable alternative fuel technology.[3,4] F-T systems currently being developed rely on natural gas as the feedstock for synthesis gas (CO/H_2), and intense scrutiny is also being given to indirect liquefaction, where coal is the source.[3] The direct conversion of natural gas to fuels will ultimately be the most desirable use of this abundant resource,[4] but recent F-T routes represent feasible, competitive substitutes, and some are actually approaching commercialization. Homogeneously catalyzed reactions,[2] and heterogeneous systems exhibiting a strong metal–support interaction,[5,6] manifest a greater inherent selectivity, suggesting that further modification of the F-T process may eventually lead to the production of oxygenated commodity chemicals. In order to take advantage of the intrinsic potential

† Present address: E. I. du Pont de Nemours & Co., Inc., Central Research and Development, Experimental Station, Wilmington, DE 19898.

(1) (a) Falbe, J. *Chemical Feedstocks from Coal*; John Wiley and Sons: New York, 1981. (b) Keim, E., Ed. *Catalysis in C_1 Chemistry*; D. Reidel: Dordrecht, The Netherlands, 1983. (c) Anderson, R. B. *The Fischer-Tropsch Synthesis*; Academic: New York, 1984. (d) Anderson, J. R.; Boudart, M. *Catalysis*; Springer-Verlag: Berlin, 1981; Vol. I. (e) Bell, A. T. *Catal. Rev.-Sci. Eng.* **1981**, *23*, 203–232. (f) Biloen, P.; Sachtler, W. M. H. *Adv. Catal.* **1981**, *30*, 165–216. (g) Rofer-DePoorter, C. K. *Chem. Rev.* **1981**, *81*, 447–474. (h) Snel, R. *Catal. Rev.-Sci. Eng.* **1987**, *29*, 361–445. (i) Wojciechowski, B. W. *Ibid.* **1988**, *30*, 629–702.

(2) (a) Dombek, B. D. *Adv. Catal.* **1983**, *32*, 325–416. (b) Lee, G. v. d.; Ponec, V. *Catal. Rev.-Sci. Eng.* **1987**, *29*, 183–218. (c) Poels, E. K.; Ponec, V. *Catalysis*; Specialist Periodic Reports; Chemical Society: London, 1983; Vol. 6, p 196.

(3) Haggin, J. *Chem. Eng. News* **1990**, *68*, July 23, 27–31.

(4) (a) Haggin, J. *Chem. Eng. News* **1992**, *70*, April 27, 33–35. (b) Haggin, J. *Ibid.* **1992**, *70*, May 4, 24–25.

0002-7863/93/1515-5570$04.00/0

of F-T technology, research into the fundamental chemistry and processing of syngas conversions will be ongoing well into the 21st century.

Our comprehension of the F-T process is derived from heterogeneous catalysis studies, surface science investigations, and homogeneous organometallic models that have generated a detailed, basic understanding of the microscopic steps involved in the reductive cleavage of carbon monoxide. A general mechanism for the sequence of reactions that make up the F-T process,[7] shown here for a typical carbon monoxide reduction and homologation on a surface,

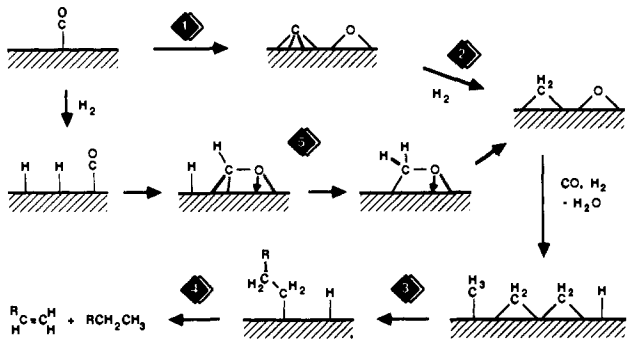

consists of four critical steps, albeit with some variation: (1) surface-adsorbed carbon monoxide ($(CO)_{ads}$)[8] dissociates via numerous proposed schemes to surface carbide (C_{ads}) and oxide (O_{ads}) or H_2O;[9-15] (2) surface hydrides formed upon chemisorption of dihydrogen transfer to the C_{ads}, producing methylidyne (CH_{ads}), methylene ($(CH_2)_{ads}$), and methyl ($(CH_3)_{ads}$) fragments,[16-19] and to any O_{ads}, forming water;[20] (3) alkyl ($(CH_2R)_{ads}$) chains grow through oligomerization of $(CH_2)_{ads}$ units;[16-20] (4) reductive elimination of a surface alkyl and hydride or β-elimination from $(CH_2CH_2R)_{ads}$ releases product alkane or olefin, respectively, upon desorption.[21] This sequence of transformations is essentially the same as that postulated by Fischer and Tropsch in 1926, with minor modifications.[7] A possible major variant (5) concerns the transfer of hydride to CO prior to dissociation,[22] a process that may aid in the stepwise degradation of the C–O bond.

Organometallic reactivity relevant to the dissociative cleavage of CO is observed for carbonyl clusters[14,15] and low-valent early transition metal species,[9-12] but external reagents are often needed to form C–H and C–C bonds from the resulting carbides. Conversely, early transition metal and actinide hydride complexes model CO reduction and C–C-bond-forming reactions,[23] yet few examples of C–O bond scission have been observed.[23-26] Homogeneously catalyzed oxygenate formation has been accomplished, but the late metal carbonylate based catalysts fail to mediate deoxygenation reactions.[2] Methylene homologation has also been evidenced in late metal binuclear systems, but these ligands are typically not derived from CO and H_2 or metal hydrides.[19]

Recently, the use of $^tBu_3SiO^-$ (silox)[27] has enabled the preparation of a series of electrophilic mono- and binuclear tantalum hydride complexes[28] capable of reducing carbon monoxide.[29] Compounds containing hard, electronegative oxygen donors such as alkoxides and siloxides in combination with hydride ligands remain rare;[30,31] related tantalum hydrides containing

(5) (a) Baker, R. T., Tauster, S. J., Dumesic, J. A., Eds. *Strong Metal-Support Interactions*; ACS Symposium Series 298; American Chemical Society: Washington, D.C., 1986. (b) Imelik, B., Ed. *Metal-Support and Metal Additive Effects in Catalysis*; Elsevier: Amsterdam, 1982.

(6) (a) Tauster, S. J. *Acc. Chem. Res.* **1987**, *20*, 389–394. (b) Tauster, S. J.; Fung, S. C.; Baker, R. T. K.; Horsley, J. A. *Science* **1981**, *211*, 1121–1125. (c) Sanchez, M. G.; Gazquez, J. L. *J. Catal.* **1987**, *104*, 120–133. (d) Sadeghi, H. R.; Henrich, V. E. *Ibid.* **1988**, *109*, 1–11. (e) Resasco, D. E.; Weber, R. S.; Sakellson, S.; McMillan, M.; Haller, G. L. *J. Phys. Chem.* **1988**, *92*, 189–193.

(7) (a) Fischer, F.; Tropsch, H. *Chem. Ber.* **1926**, *59*, 830–836. (b) Craxford, S. R.; Rideal, E. K. *J. Chem. Soc.* **1939**, 1604–1614.

(8) Sung, S.-S.; Hoffmann, R. *J. Am. Chem. Soc.* **1985**, *107*, 578–854 and references cited therein.

(9) Neithamer, D. R.; LaPointe, R. E.; Wheeler, R. A.; Richeson, D. S.; Van Duyne, G. D.; Wolczanski, P. T. *J. Am. Chem. Soc.* **1989**, *111*, 9056–9072 and references cited therein.

(10) Chisholm, M. H.; Hammond, C. E.; Johnston, V. J.; Streib, W. E.; Huffman, J. C. *J. Am. Chem. Soc.* **1992**, *114*, 7056–7065 and references cited therein.

(11) Evans, W. J.; Grate, J. W.; Hughes, L. A.; Zhang, H.; Atwood, J. L. *J. Am. Chem. Soc.* **1985**, *107*, 3728–3730.

(12) For related CO couplings, see: (a) Berry, D. H.; Bercaw, J. E.; Jircitano, A. J.; Mertes, K. B. *J. Am. Chem. Soc.* **1982**, *104*, 4712–4715. (b) Protasiewicz, J. D.; Lippard, S. J. *Ibid.* **1991**, *113*, 6564–6570. (c) Bianconi, P. A.; Vrtis, R. N.; Rao, C. P.; Williams, I. D.; Engeler, M. P.; Lippard, S. J. *Organometallics* **1987**, *6*, 1968–1977. (d) Sherry, A. E. Wayland, B. B. *J. Am. Chem. Soc.* **1989**, *111*, 5010–5012. (e) Coffin, V. L.; Brennen, W.; Wayland, B. B. *Ibid.* **1988**, *110*, 6063–6069.

(13) (a) Low, G. G.; Bell, A. T. *J. Catal.* **1979**, *57*, 397–405. (b) Roberts, M. W. *Chem. Soc. Rev.* **1977**, *6*, 373–391. (c) Brodén, G.; Rhodin, T. N.; Brucker, C.; Benbow, R.; Hurych, Z. *Surf. Sci.* **1976**, *59*, 593–611.

(14) (a) Horwitz, C. P.; Shriver, D. F. *Adv. Organomet. Chem.* **1984**, *23*, 219–305. (b) Bradley, J. S. *Ibid.* **1983**, *22*, 1–58. (c) Muetterties, E. L.; Stein, J. *Chem. Rev.* **1979**, *79*, 479–490. (d) Tachikawa, M.; Muetterties, E. L. *Prog. Inorg. Chem.* **1981**, *28*, 203–238. (e) Kahn, B. E.; Rieke, R. D. *Chem. Rev.* **1988**, *88*, 733–745.

(15) (a) Shriver, D. F.; Sailor, M. J. *Acc. Chem. Res.* **1988**, *21*, 374–379. (b) Horwitz, C. P.; Shriver, D. F. *J. Am. Chem. Soc.* **1985**, *107*, 8147–8153.

(16) (a) Biloen, P.; Helle, J. N.; van den Berg, F. G. A.; Sachtler, W. M. H. *J. Catal.* **1983**, *81*, 450–463. (b) Biloen, P.; Helle, J. N.; Sachtler, W. M. H. *Ibid.* **1979**, *58*, 95–107. (c) Araki, M.; Ponec, V. *Ibid.* **1976**, *44*, 439–448. (d) Zhang, X.; Biloen, P. *Ibid.* **1986**, *98*, 468–476. (e) Biloen, P. *Recl. Trav. Chim. Pays-Bas* **1980**, *99*, 33–38. (f) Vannice, M. A.; Sudhaker, C. *J. Phys. Chem.* **1984**, *88*, 2429–2432. (g) Mims, C. A.; McCandlish, L. E. *Ibid.* **1987**, *91*, 929–937.

(17) (a) Brady, R. C., III; Pettit, R. *J. Am. Chem. Soc.* **1981**, *103*, 1287–1289. (b) Brady, R. C., III; Pettit, R. *Ibid.* **1980**, *102*, 6182–6184.

(18) (a) George, P. M.; Avery, N. R.; Weinberg, W. H.; Tebbe, F. N. *J. Am. Chem. Soc.* **1983**, *105*, 1393–1394. (b) Erley, W.; McBreen, P. H.; Ibach, H. *J. Catal.* **1983**, *84*, 229–234. (c) Barteau, M. A.; Feulner, P.; Stengl, R.; Broughton, J. Q.; Menzel, D. *Ibid.* **1985**, *94*, 51–59. (d) Kaminsky, M. P.; Winograd, N.; Geoffroy, G. L. *J. Am. Chem. Soc.* **1986**, *108*, 1315–1316. (e) Lee, M. B.; Yang, Q. Y.; Tang, S. L.; Ceyer, S. T. *J. Chem. Phys.* **1986**, *85*, 1693–1694.

(19) (a) Maitlis, P. M.; Saez, I. M.; Meanwell, N. J.; Isobe, K.; Nutton, A.; Váquez de Miguel, A.; Bruce, D. W.; Okeya, S.; Bailey, P. M.; Andrews, D. G.; Ashton, P. R.; Johnstone, I. R. *New J. Chem.* **1989**, *13*, 419–425. (b) Herrmann, W. A. *Adv. Organomet. Chem.* **1982**, *20*, 159–263. (c) Herrmann, W. A. *Angew. Chem., Int. Ed. Engl.* **1982**, *21*, 117–130 and references cited therein.

(20) Ekstrom, A.; Lapszewicz, J. *J. Phys. Chem.* **1984**, *88*, 4577–4580.

(21) Zheng, C.; Zpeloig, Y.; Hoffmann, R. *J. Am. Chem. Soc.* **1988**, *110*, 749–774.

(22) (a) Gladysz, J. A. *Adv. Organomet. Chem.* **1982**, *20*, 1–38. (b) Masters, C. *Ibid.* **1979**, *17*, 61–103. (c) Pichler, H.; Schulz, H. *Chem.-Ing.-Tech.* **1970**, *12*, 1160–1174.

(23) For a recent, brief review of early metal and actinide hydride CO reactivity, see: Cummins, C. C.; Van Duyne, G. D.; Schaller, C. P.; Wolczanski, P. T. *Organometallics* **1991**, *10*, 164–170.

(24) For CO cleavage reactions requiring ligand participation (e.g., hydride transfer), see: (a) Marsella, J. A.; Huffman, J. C.; Folting, K.; Caulton, K. G. *Inorg. Chem. Acta* **1985**, *96*, 161–170. (b) Marsella, J. A.; Huffman, J. C.; Folting, K.; Caulton, K. G. *J. Am. Chem. Soc.* **1981**, *103*, 5596–5598. (c) Wood, C. D.; Schrock, R. R. *Ibid.* **1979**, *101*, 5421–5422. (d) Planalp, R. P.; Andersen, R. A. *Ibid.* **1983**, *105*, 7774–7775. (e) Blenkers, J.; de Liefde Meijer, H. J.; Teuben, J. H. *Organometallics* **1983**, *2*, 1483–1484. (f) Shapley, J. R.; Park, J. T.; Churchill, M. R.; Ziller, J. W.; Beanan, L. R. *J. Am. Chem. Soc.* **1984**, *106*, 1144–1145. (g) Jacobsen, E. N.; Trost, M. K.; Bergman, R. G. *Ibid.* **1986**, *108*, 8092–8094. (h) Meyer, T.; Messerle, L. *Ibid.* **1990**, *112*, 4564–4565.

(25) Thermal deoxygenation events have been observed in zirconium systems. See: (a) Erker, G.; Dorf, U.; Atwood, J. L.; Hunter, W. E. *J. Am. Chem. Soc.* **1986**, *108*, 2251–2257. (b) Erker, G.; Schlund, R.; Albrecht, M.; Sarter, C. *J. Organomet. Chem.* **1988**, *353*, C27–29. (c) Erker, G. *Acc. Chem. Res.* **1984**, *17*, 103–109 and references cited therein.

(26) For similar deoxygenation of ketones and aldehydes, see: (a) Bryan, J. C.; Mayer, J. M. *J. Am. Chem. Soc.* **1990**, *112*, 2298–2308. (b) Chisholm, M. H.; Folting, K.; Klang, J. A. *Organometallics* **1990**, *9*, 602–606. (c) Neithamer, D. R., Ph.D. Thesis, Cornell University, Ithaca, NY, 1989.

(27) (a) Weidenbruch, M.; Pierrard, C.; Pesel, H. *Z. Naturforsch. B: Anorg. Chem. Org. Chem.* **1978**, *33B*, 1468–1471. (b) Dexheimer, E. M.; Spialter, L.; Smithson, L. D. *J. Organomet. Chem.* **1975**, *102*, 21–27.

(28) LaPointe, R. E.; Wolczanski, P. T. *J. Am. Chem. Soc.* **1986**, *108*, 3535–3537 and references cited therein.

(29) Toreki, R.; LaPointe, R. E.; Wolczanski, P. T. *J. Am. Chem. Soc.* **1987**, *109*, 7558–7560.

(30) For recent alkoxy hydrides, see: (a) Ankianiec, B. C.; Fanwick, P. E.; Rothwell, I. P. *J. Am. Chem. Soc.* **1991**, *113*, 4710–4712. (b) Profilet, R. D.; Fanwick, P. E.; Rothwell, I. P. *Polyhedron*, in press.

Table I. NMR (δ in ppm (m, J in Hz))[a] and IR (cm^{-1})[b] Data for Monomeric Hydrides $(silox)_nTaHX$ and Carbonylation Products

compound	^1H[c] silox	^1H[c] TaH	^1H[c] other	^{13}C or $^{13}C\{^1H\}$[d] $Si(C(CH_3)_3)_3$	^{13}C or $^{13}C\{^1H\}$[d] other	$^{29}Si\{^1H\}$[e] silox/other	IR TaH/D[e]
$(silox)_3TaH_2$ (**2**)[f]	1.26	21.99		23.37		15.29[g]	1725/1250
$(silox)_3TaHD$ (**2**-d_1)		21.97		30.49			750/570[h]
$(silox)_2HTaOSi^tBu_2CMe_2CH_2$ (**4**)[i]	1.27	21.97	1.29 (^{t}Bu) 1.37 (Me_2) 1.89 (br, CH_2)	23.61 30.73	23.52 (SiC) 24.93 ($SiCMe_2$) 33.61 ($C(CH_3)_3)_2$ 39.80 ($CCH_3)_2$) 97.04 (CH_2)	16.37 20.43	1770
$(silox)_3HTaEt$ (**5**)	1.29	22.29 (t, 3.2)	1.82 (dq, 3.2, 7.8) 2.17 (t, 7.8)	23.69 30.76 (q, 126)	16.44 (q, 125) 70.90 (t, 119)		1794
$(silox)_3HTaCl$ (**6**-Cl)	1.30	20.08					1741
$(silox)_3HTaI$ (**6**-I)	1.32	17.95					1746
$[(silox)_3TaH]_2(\mu:\eta^1,\eta^1\text{-}CH_2(CH_2)_3O)$ (**7**)	1.30 1.33	21.17 22.38 (t, 3)	1.84 (CH_2, ddd; 3,7,8) 1.97 (CH_2, m, 7) 2.37 ($TaCH_2$, m) 4.67 (OCH_2, dd; 7,8)	23.71 30.78	27.76 (CH_2) 31.52 (CH_2) 40.89 (CH_2) 77.12 (CH_2)		1800
$(silox)_3Ta(\eta^2\text{-}OCH_2)$ (**15**)	1.25		4.06	23.56 30.58	93.87 (t, 159)		*j*
$(silox)_3Ta(\eta^2\text{-}OCHEt)$ (**17**)[k]	1.27		1.35 (Me, t, 7.1) 2.22 (C*H*H, ddq; 9.6, 14, 7.1) 2.27 (CH*H*, ddq; 3.3, 14, 7.1) 4.46 (CHEt, dd; 3.3, 9.6)	23.57 30.61 (q, 126)	17.15 (q, 126) 111.67 (d, 152)		

[a] Benzene-d_6 unless otherwise noted. [b] Nujol unless otherwise noted. [c] Referenced to Me_4Si at δ 0.0 or benzene-d_6 at δ 7.15. [d] Referenced to benzene-d_6 at δ 128.00. [e] Broad ν(Ta-H/D) unless otherwise noted. [f] From ref 9. [g] Selective decoupling experiments indicated $J_{SiH(Ta)} \approx 0$. [h] Assigned to scissoring mode, $\delta(TaH_2/D_2)$; very strong. [i] From ref 37; tentative $^{13}C\{^1H\}$ and $^{29}Si\{^1H\}$ assignments based on intensity. [j] IR (**15**/**15**-d_2/**15**-^{13}C, cyclohexane) $\nu(H_2CO/D_2CO/H_2{}^{13}CO)$ 932/932/914, ($CH_2/CD_2/{}^{13}CH_2$ wag) 552, 502, 543, ($H_2CO/D_2CO/H_2{}^{13}CO$ rock (tentative)) 600, 588, 600 cm^{-1}. [k] Methylene not located in ^{13}C NMR.

softer ancillary ligands are unable to effect the breakdown of CO.[32,33] Described herein is the final report concerning the syntheses and carbonylation chemistry of numerous silox hydrides of tantalum, with a special focus on the reactivity of $[(silox)_2TaH_2]_2$,[29] whose structure has been determined by X-ray crystallography. Carbonylation of this binuclear complex results in C–O bond cleavage, C–H bond formation, and carbon–carbon coupling reactions that model the critical bond-making and bond-breaking steps in F-T synthesis.

Results

Synthesis and Characterization. 1. Monomeric Hydrides. Monomeric tantalum hydrides were prepared by taking advantage of the bulky tris-silox coordination sphere about $(silox)_3TaCl_2$ (**1**),[9] a convenient starting material. Table I lists spectroscopic details of the hydride complexes,[34] and Scheme I illustrates the preparative chemistry, which centers around clean reduction of the dichloride (**1**) without the loss of a silox ligand.[35] In these sections, all gas uptake and release measurements were conducted via Toepler pump methods.

Sodium amalgam reduction of **1** in THF under dihydrogen afforded $(silox)_3TaH_2$ (**2**) in 43% yield after crystallization from hexanes, but the dihydride was typically prepared in ~80% yield from addition of H_2 to $(silox)_3Ta$ (**3**), as previously described.[9] The composition of trigonal bipyramidal **2** was checked by exposure to 2 equiv of HCl, yielding dichloride **1** (>95%) and 1.8 equiv of H_2. Extended thermolysis (100 °C, 6 days) of **2** (^1H NMR δ 21.99 (TaH_2); IR ν(TaH/D) = 1725/1250, $\delta(TaH_2/D_2)$ = 750/570 cm^{-1}) in a sealed NMR tube caused cyclometalation[36] to $(silox)_2HTaOSi^tBu_2CMe_2CH_2$ (**4**: δ 21.97 (TaH); ν(TaH) = 1770 cm^{-1}),[37] but the dihydride could be reconstituted upon heating **4** for 6 days under 3 atm of dihydrogen. This reversible process probably occurs via a σ-bond metathesis pathway, but critical labeling experiments that distinguish this mechanism from a standard oxidative addition/reductive elimination process[38] are obviated by rapid dihydrogen/TaH exchange (*vide infra*).

Treatment of $(silox)_3TaH_2$ (**2**) with a 2-fold excess of ethylene provided colorless crystals of $(silox)_3HTaEt$ (**5**) in 63% yield upon crystallization from hexanes. A C_{3v} structure was assigned to **5** on the basis of steric arguments and a 3.2-Hz coupling between the TaH (δ 22.29) and $TaCH_2$ (δ 1.82) units. Although ethyl hydride **5** is electronically unsaturated, an agostic[39] methylene interaction was not evidenced in the ^{13}C NMR spectrum (J_{CH} = 119 Hz), and reaction with additional ethylene did not occur. Since the spectral features of **5**, including the hydride stretch (ν(TaH) = 1794 cm^{-1}), proved to be ordinary, the failure to

(31) For recent, multinuclear alkoxy hydrides, see: (a) Chisholm, M. H.; Kramer, K. S.; Streib, W. E. *J. Am. Chem. Soc.* **1992**, *114*, 3571–3573. (b) Chacon, S. T.; Chisholm, M. H.; Folting, K.; Hampden-Smith, M. J.; Huffman, J. C. *Inorg. Chem.* **1991**, *30*, 3122–3125. (c) Chisholm, M. H.; Huffman, J. C.; Smith, C. A. *J. Am. Chem. Soc.* **1986**, *108*, 222–230. (d) Akiyama, M.; Chisholm, M. H.; Cotton, F. A.; Extine, M. W.; Haitko, D. A.; Leonelli, J.; Little, D. *Ibid.* **1981**, *103*, 779–784. (e) Hoffman, D. M.; Lappas, D.; Wierda, D. A. *Ibid.* **1989**, *111*, 1531–1533. (f) Mayer, J. M.; Wolczanski, P. T.; Santarsiero, B. D.; Olson, W. A.; Bercaw, J. E. *Inorg. Chem.* **1983**, *22*, 1149–1155.

(32) For example, see: Scioly, A. J.; Luetkens, M. L.; Wilson, R. B., Jr.; Huffman, J. C.; Sattelberger, A. P. *Polyhedron* **1987**, *6*, 741–757.

(33) For a related hydride carbonylation, see: (a) Belmonte, P. A.; Cloke, F. G. N.; Schrock, R. R. *J. Am. Chem. Soc.* **1983**, *105*, 2643–2650. (b) Churchill, M. R.; Wasserman, H. J. *Inorg. Chem.* **1982**, *21*, 226–230.

(34) Bercaw and co-workers have observed an upfield shift of the ^1H NMR hydride resonances in Cp^*_2MHX (M = Zr, Hf) with increasing π-donor ability of X, but an analogous trend is not evident in this system. See: Roddick, D. M.; Fryzuk, M. D.; Seidler, P. F.; Hillhouse, G. L.; Bercaw, J. E. *Organometallics* **1985**, *4*, 97–104.

(35) (a) Covert, K. J.; Wolczanski, P. T.; Hill, S. A.; Krusic, P. J. *Inorg. Chem.* **1992**, *31*, 66–78. The compatability of the silox group with a reduced metal center has been interpreted herein as being due to a combination of its electronegative properties as an oxygen donor and its diminished capacity for $O(p\pi) \rightarrow M(d\pi)$ donation, perhaps due to an increased $O(p\pi) \rightarrow Si(d\pi)$ interaction. In contradiction, recent *ab initio* calculations failed to support the notion of silicon–oxygen π-bonding. See: (b) Shambayate, S.; Blake, J. F.; Wierschke, S. G.; Jorgensen, W. L.; Schreiber, S. L. *J. Am. Chem. Soc.* **1990**, *112*, 697–703.

(36) For general references on cyclometalation in early transition metal systems, see: (a) Rothwell, I. P. *Polyhedron* **1985**, *4*, 177–200. (b) Rothwell, I. P. *Acc. Chem. Res.* **1988**, *21*, 153–159.

(37) Covert, K. J.; Neithamer, D. R.; Zonnevylle, M. C.; LaPointe, R. E.; Schaller, C. P.; Wolczanski, P. T. *Inorg. Chem.* **1991**, *30*, 2494–2508.

(38) The intermediacy of $(silox)_3Ta$ (**3**) is plausible, since independent rate measurements of its cyclometalation to **4** revealed it to be faster (~12 h, 70 °C, ref 37) than the corresponding reaction of **2**. A kinetics investigation (i.e., $[H_2]$-dependence studies) was not attempted.

(39) (a) Brookhart, M.; Green, M. L. H.; Wong, L. *Prog. Inorg. Chem.* **1988**, *36*, 1–124. (b) Brookhart, M.; Green, M. L. H. *J. Organomet. Chem.* **1983**, *250*, 395–408.

Scheme I

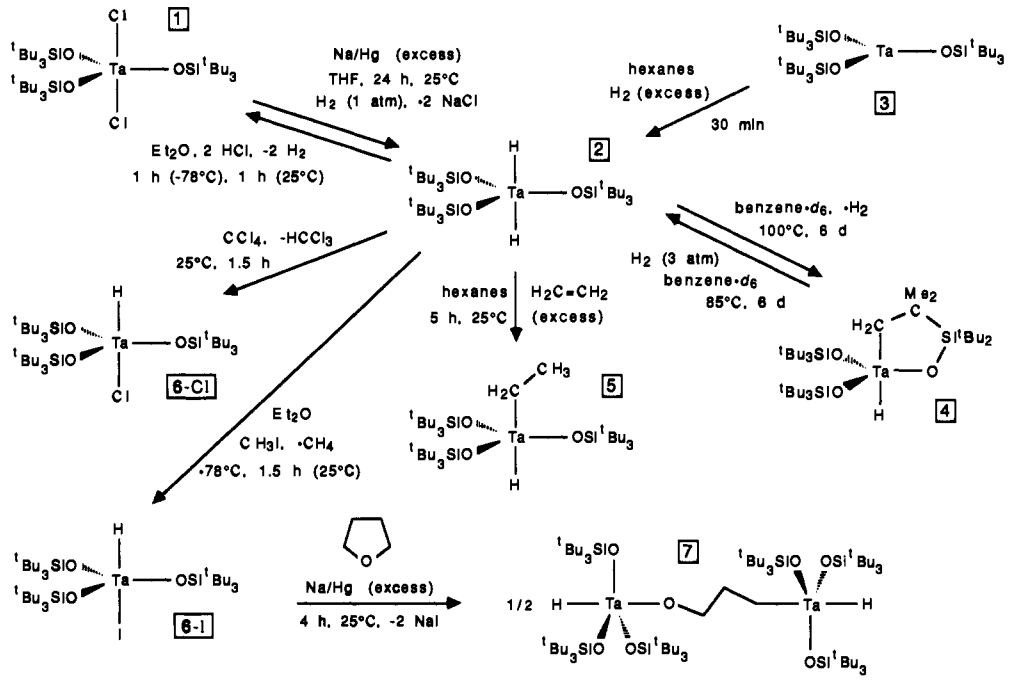

observe a second ethylene insertion is ascribed to the increased steric bulk of the alkyl hydride. While formation of a diethyl species is expected to be favorable according to bond strength arguments (i.e., $MH + C_2H_4$, $\Delta H < 0$),[40] the steric requirements of the ancillary ligands may destabilize this derivative or raise the barrier to insertion.

Hydrido halide derivatives were prepared by exposure of $(silox)_3TaH_2$ (**2**) to neat CCl_4 and an ethereal solution of CH_3I, yielding colorless $(silox)_3HTaCl$ (**6**-Cl) and $(silox)_3HTaI$ (**6**-I) in 63% and 62% yields, respectively, upon crystallization from hexanes. Both complexes exhibited characteristic downfield hydride chemical shifts and broad, relatively low energy TaH stretching modes (**6**-Cl: δ 20.08, ν(TaH) = 1741 cm^{-1}; **6**-I: δ 17.95, ν(TaH) = 1746 cm^{-1}). While the reduction of CH_3I is a standard method for the conversion of early metal hydrides to iodides,[41] the clean conversion of **2** to **6**-Cl with CCl_4 was rather surprising. Exposure of **2** to 1 equiv of HCl, CH_3Cl, or CH_2Cl_2 led to less discriminate reactivity, including formation of $(silox)_3TaCl_2$ (**1**), indicating further reaction of **6**-Cl. In comparison, carbon tetrachloride is predicted to be more prone to reduction, but its relatively greater size may enable it to react preferentially with dihydride **2**, rather than the larger hydrochloride (**6**-Cl).

The steric influence of the tris-silox coordination sphere on the above transformations suggested that synthesis of a Ta(IV) hydride was possible. Reduction of $(silox)_3HTaI$ (**6**-I) with an excess of Na/Hg in THF produced an emerald green solution that faded to yellow over a 4-h period. A compound containing a ring-opened THF, $[(silox)_3TaH]_2(\mu{:}\eta^1,\eta^1\text{-}CH_2(CH_2)_3O)$ (**7**), was isolated as an off-white powder in 58% yield. A single, broad IR band at 1800 cm^{-1} corroborated the existence of two hydrides, which were observed at δ 21.17 and 22.38 in the ^1H NMR spectrum, the latter coupled (t, J_{HH} = 3 Hz) to the tantalum methylene. Two distinct silox proton singlets revealed the independent tantalums, while the ^1H and $^{13}C\{^1H\}$ NMR spectra exhibited four different methylene resonances for the five-atom bridge. Analogous features are observed for $[(silox)_3Ti]_2(\mu{:}\eta^1,\eta^1\text{-}CH_2(CH_2)_3O)$, a ring-opened product derived from exposure of d^1 $(silox)_3Ti$ to THF.[42] It is plausible that d^1 $(silox)_3TaH$ (**6**) is formed upon reduction, but is ultimately scavenged by THF to give **7**. Further attempts to isolate **6** were unsuccessful.

2. Dimeric Hydrides. Attempts to generate hydride derivatives via the high-pressure hydrogenation of tantalum alkyl species[30] proved unsuccessful,[43] although one notable exception foreshadowed the synthesis of dimeric hydride complexes. Since relatively weak metal–benzyl bonds should be more susceptible to hydrogenation, canary yellow $(silox)_2Cl_2TaCH_2Ph$ (**8**)[44] was treated with 3 atm of H_2 in benzene-d_6, but 80 °C thermolysis (~4 h) failed to initiate a reaction. In contrast, photolysis of **8** under 3 atm of H_2 effected a smooth conversion to $(silox)_2TaCl_3$ (**9**)[44] and purple $[(silox)_2TaCl]_2(\mu\text{-}H)_2$ (**10**), with concomitant formation of toluene and a trace amount of bibenzyl (eq 1). While

$$(silox)_2Cl_2TaCH_2Ph \;(\mathbf{8}) \xrightarrow[C_6D_6,\ 25\ ^\circ C]{H_2\ (3\ atm),\ h\nu} {}^1/_2(silox)_2TaCl_3\ (\mathbf{9}) + {}^1/_4[(silox)_2TaCl]_2(\mu\text{-}H)_2\ (\mathbf{10}) + C_7H_8 + PhCH_2CH_2Ph\ (\text{trace, } <5\%) \quad (1)$$

several mechanistic possibilities can be envisioned, photolytic cleavage of the $TaCH_2Ph$ probably initiates the reaction.[45] Most importantly, hydrochloride dimer **10** contains two Ta(IV) fragments, suggesting that the reduction of **9** under dihydrogen would lead to formation of bis-silox hydride derivatives.

The preparation of dimeric Ta(IV) hydrides is depicted in Scheme II, and their spectral characteristics are given in Table II. Treatment of $(silox)_2TaCl_3$ (**9**) with excess Na/Hg under 1 atm of dihydrogen for ~15 days afforded orange $[(silox)_2TaH_2]_2$ (**11**) in 83% yield upon crystallization from diethyl ether. After about 5 days, the toluene solution was the deep purple color attributed to $[(silox)_2TaCl]_2(\mu\text{-}H)_2$ (**10**), but ^1H NMR analysis of an aliquot revealed the presence of both **10** and **11**. The extended time period was necessary to convert all of the remaining **10** to the tetrahydride **11** and to destroy interfering byproducts.

(40) Schock, L. E.; Marks, T. J. *J. Am. Chem. Soc.* **1988**, *110*, 7701–7715 and references cited therein.

(41) For examples, see: (a) Manriquez, J. M.; McAlister, D. R.; Sanner, R. D.; Bercaw, J. E. *J. Am. Chem. Soc.* **1978**, *100*, 2716–2724. (b) Barger, P. T.; Santarsiero, B. D.; Armantrout, J.; Bercaw, J. E. *J. Am. Chem. Soc.* **1984**, *106*, 5178–5186.

(42) Covert, K. J. Ph.D. Thesis, Cornell University, Ithaca, NY, 1991.

(43) LaPointe, R. E. Ph.D. Thesis, Cornell University, Ithaca, NY, 1986.

(44) LaPointe, R. E.; Wolczanski, P. T.; Van Duyne, G. D. *Organometallics* **1985**, *4*, 1810–1818.

(45) For leading references ($PhCH_2^{\bullet}$), see: Daikh, B. E.; Finke, R. G. *J. Am. Chem. Soc.* **1992**, *114*, 2938–2943.

Scheme II

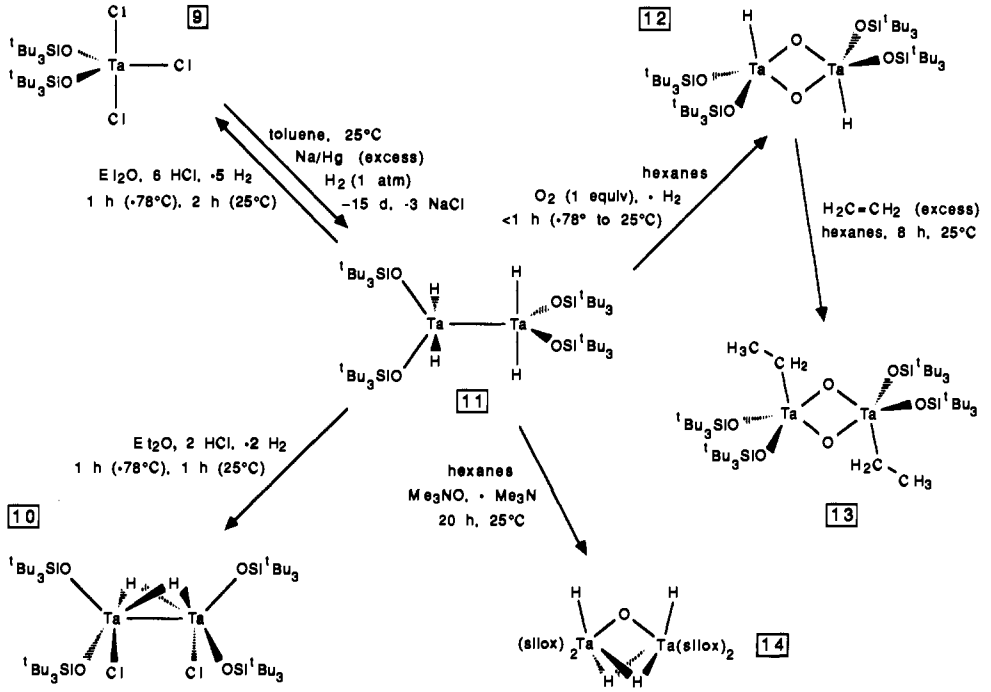

Table II. NMR (δ in ppm (m, J in Hz))[a] and Pertinent IR (cm^{-1})[b] Data for $[(silox)_2TaH_2]_2$ and Derivatives

	^1H[c]			^{13}C or $^{13}C\{^1H\}$[d]			$^{29}Si\{^1H\}$[c]	
compound	silox	TaH	other	silox (SiC)	$(C(CH_3)_3)_3$	other	silox/other	IR TaH/D[e]
$[(silox)_2TaH_2]$ (**11**, 25 °C)	1.25	12.15		23.27	30.34		14.14[f]	1792/1283
(**11**, -80 °C)[g,h]		12.06					12.11[i]	
$[(silox)_2TaCl]_2(\mu\text{-}H)_2$ (**10**)	1.27	9.35		23.81	30.78		16.75	1595/1240
				24.25			19.32	
$[(silox)_2TaH]_2(\mu\text{-}O)_2$ (**12**)	1.28	20.67		23.48	30.25			1808/1297[j]
$[(silox)_2TaCH_2CH_3]_2(\mu\text{-}O)_2$ (**13**)	1.30 (br)		2.15 (CH_2, q, 7)	23.83	30.69	16.95 (q, 130)		
			2.26 (CH_3, t, 7)		(q, 126)	61.31 (t, 122)		
$[(silox)_2TaH]_2(\mu\text{-}H)_2(\mu\text{-}O)$ (**14**, 40 °C)	1.27	14.83					14.84	1834/1313
								1779/1275
								1345/985[k]
(**14a**, -105 °C)[h]		9.51					13.9[l]	
		19.04					15.0[l]	
(**14b**, -80 °C)[h]		9.85					12.73	
		19.39					13.59	

[a] Benzene-d_6 unless otherwise noted. [b] Nujol unless otherwise noted. [c] Referenced to Me_4Si at δ 0.0 or benzene-d_6 at δ 7.15. [d] Referenced to benzene-d_6 at δ 128.00. [e] Broad ν(TaH/D) unless otherwise noted. [f] Selective decoupling experiments indicated $J_{SiH(Ta)} \approx 0$. [g] Toluene-d_8. [h] Silox groups broadened due to slow rotation. [i] Toluene-d_8, -70 °C. [j] Hexanes, $\nu(Ta^{16}O/^{18}O)$ 921/883, 803/766, 704/674 cm^{-1}. [k] Very broad ($\nu_{1/2} \approx 100$ cm^{-1}). [l] Tentative assignments on signals barely base-line resolved; averaged signal at -80 °C was δ 14.76.

Concentration of the toluene solution (typically ~0.3 M) also accelerated the reduction process. In the absence of water and O_2, tetrahydride **11** melts at 180 °C, distills at 220 °C ($\sim 10^{-4}$ Torr), and is indefinitely stable in hydrocarbon and ethereal solvents. The composition of **11** was checked via exposure to 6 equiv of HCl in Et_2O; $(silox)_2TaCl_3$ (**9**) was regenerated, according to ^1H NMR analysis (>95%), and 4.8 equiv of H_2 was released.

Molecular weight measurements, a single-crystal X-ray diffraction experiment (*vide infra*), and spectroscopic studies revealed the dimeric, D_{2d} conformation of $[(silox)_2TaH_2]_2$ (**11**). An unbridged Ta–Ta bond interlocks two trigonal bipyramids containing axial hydrides and equatorial silox groups. Single resonances were found for the silox (^1H, $^{13}C\{^1H\}$, and $^{29}Si\{^1H\}$ NMR (-70 °C, toluene-d_8)) and hydride (C_6D_6, δ 12.15) ligands, and the latter remained unchanged from 25 to -80 °C in toluene-d_8 (δ 12.06). In the IR spectrum, a broad, terminal Ta–H(D) stretch was observed at 1792(1283) cm^{-1}, and no other bands shifted upon labeling with deuterium.

Exposure of $[(silox)_2TaH_2]_2$ (**11**) to 2.0 equiv of HCl caused the evolution of 2.0 equiv of dihydrogen and generated violet $[(silox)_2TaCl]_2(\mu\text{-}H)_2$ (**10**), which was isolated in 78% yield upon crystallization from THF. The hydrochloride dimer is postulated to contain two bridging hydrides on the basis of a ν(TaH) at 1595 cm^{-1} in its IR spectrum. Related to this, crystallographically characterized $(\eta^5\text{-}C_5R_5)_2Ta_2Cl_3R'(\mu\text{-}H)_2$ (R' = alkyl, Cl) species prepared by Schrock and co-workers possess a similar spectral feature.[33] The lone hydride resonance at δ 9.35 in the ^1H NMR spectrum and inequivalent silox groups in $^{13}C\{^1H\}$ and $^{29}Si\{^1H\}$ NMR spectra are consistent with a C_{2h} metal–metal-bonded structure of $(\mu\text{-}H)_2$-linked trigonal bipyramids with axial and equatorial silox groups or a C_2 structure of two square pyramids linked by the Ta–Ta bond and basal μ-H bridges. Because of the analogy to $(\eta^5\text{-}C_5H_5)_2Ta_2Cl_3R'(\mu\text{-}H)_2$, the C_2 geometry is slightly preferred.

When 1.0 equiv of dioxygen was added to $[(silox)_2TaH_2]_2$ (**11**) in hexanes, 0.91 equiv of H_2 was evolved, and $[(silox)_2TaH]_2(\mu\text{-}O)_2$ (**12**) was isolated quantitatively upon removal of the solvent. Colorless **12** is dimeric according to molecular weight measurements, and its ^1H NMR spectrum exhibited single resonances for the silox and hydride (δ 20.67) ligands. A typical terminal hydride(deuteride) IR stretch was observed at 1808(1297) cm^{-1}, while the Ta_2O_2 core displayed three bands at 921, 803, and 704

cm^{-1} that shifted to 883, 766, and 674 cm^{-1}, respectively, upon ^{18}O substitution. It is interesting that absorptions attributed to the μ-O group are energetically close to the terminal Ta=O stretches of $Cp^*_2Ta{=}O(H)$ (850 cm^{-1})[46] and $(silox)_3Ta{=}O$ (905 cm^{-1}),[9] indicating substantial multiple bond character.[47] Considering steric arguments, a structure consisting of two trigonal bipyramids linked by oxos that occupy an axial site on one metal and an equatorial site on another appears most reasonable.

The oxo hydride dimer **12** was derivatized via the addition of excess ethylene to provide colorless $[(silox)_2TaCH_2CH_3]_2(\mu\text{-}O)_2$ (**13**) upon crystallization from Et_2O. The low isolated yield (39%) of the oxo ethyl dimer (**13**) was due to its high solubility, because the reaction appeared quantitative by NMR. Molecular weight measurements were consistent with a dimer; thus, the structure of **13** is considered analogous to that of **12**.

Treatment of $[(silox)_2TaH_2]_2$ (**11**) with Me_3NO, an oxygen atom source, produced $[(silox)_2TaH]_2(\mu\text{-}H)_2(\mu\text{-}O)$ (**14**) over a 3-h period. Colorless crystals of **14** were isolated in 67% yield upon crystallization from diethyl ether. The extended reaction time is believed to be a consequence of the low solubility of the *N*-oxide. Above room temperature, the ^1H NMR spectrum of **14** belied its bridging hydride structure, because the hydrides resonated as a singlet at δ 14.83. Low-temperature NMR spectra exhibited a complexity that suggested the existence of a bridging hydride structure(s) for **14**, and deuterium substitution confirmed a very broad $Ta_2(\mu\text{-}H)$ band at 1345 cm^{-1} ($\nu_{1/2} \approx 100$ cm^{-1}) in the IR spectrum, in addition to terminal ν(TaH) absorptions at 1834 and 1799 cm^{-1}.

Variable-Temperature NMR Experiments on $[(silox)_2TaH]_2(\mu\text{-}H)_2(\mu\text{-}O)$ (14). Variable-temperature ^1H and $^{29}Si\{^1H\}$ NMR spectra of $[(silox)_2TaH]_2(\mu\text{-}H)_2(\mu\text{-}O)$ (**14**) revealed the presence of two fluxional, interconvertible isomers in approximately equal concentrations. Only one resolvable ^1H NMR resonance was observed for the silox ligands at all temperatures studied, with substantial low-temperature broadening attributed to hindered rotation of the ^{t}Bu groups.[44] Species **14a** exhibited 1:1 hydride resonances at δ 9.51 and δ 19.04 at the low-temperature limit of −100 °C in methylcyclohexane-d_{14}, while species **14b** possessed 1:1 singlets at δ 9.85 and δ 19.39, indicative of a similar structure. Upon generation of **14** from $(silox)_4Ta_2D_nH_{4-n}$ (n = 0–4, **11**-d_n), the intensities of the signals at δ 9.51 and δ 9.85 decreased relative to those at lower field, consistent with preferential occupation of the terminal (upfield) sites by deuterium.[48-50] The resonances attributed to **14a** coalesced at −85 °C ($\Delta G^\ddagger$ = 8.0 kcal/mol, $k = 4.2 \times 10^3$ s^{-1}), and activation parameters of $\Delta H^\ddagger$ = 9.1(4) kcal/mol and $\Delta S^\ddagger$ = 6(3) eu were obtained by fitting the line shapes at four temperatures (−100 to −50 °C). At temperatures greater than −70 °C, the hydride resonances of **14b** broadened and coalesced at ~5 °C as they merged with the averaged signal of **14a**. At this temperature, the activation energy for the interconversion of **14a** with **14b** was estimated to be $\Delta G^\ddagger \approx 11.6$ kcal/mol ($k = 4.2 \times 10^3$ s^{-1}).

The variable-temperature $^{29}Si\{^1H\}$ NMR data corroborated these findings. At −105 °C, two $^{29}Si\{^1H\}$ signals attributed to **14b** at δ 12.73 and 13.59 were observed, and two broadened singlets at roughly δ 13.9 and 15.0 were assigned to **14a**. At temperatures from −90 to −60 °C, an averaged resonance for **14a** at δ 14.76 first sharpened and then began to broaden along with the signals attributed to **14b**. At ca. −40 °C the resonances of both isomers coalesced, and the sharp singlet (δ 14.84) observed at 20 °C revealed a rapid interchange of isomers. If the coalescence of the signals ascribed to **14a** is estimated to occur at −100 °C, the $\Delta G^\ddagger$ ($k \approx 1.8 \times 10^2$ s^{-1}) for averaging the silox groups is ~8.2 kcal/mol. Similarly, the coalescence observed at −40 °C can be used to estimate the activation energy ($\Delta G^\ddagger \approx 11$ kcal/mol, $k \approx 2.8 \times 10^2$ s^{-1}) for interconversion of **14a** with **14b**.

The data clearly indicate an independent averaging process for **14a**, while the fluxionality ascribed to **14b** is less well defined. Specifically, it proved difficult to determine which barrier was larger: equilibration of **14a** with **14b** or an independent averaging of the bridge and terminal sites on **14b**. This ambiguity was eliminated by obtaining a direct mapping of the exchange network between the multiple sites, using the two-dimensional exchange spectroscopy (EXSY) experiment.[51,52] The experiment measures the transfer of magnetization due to chemical exchange during a mixing time, τ_m. Using a very short mixing time (τ_m = 1 ms),[53] cross-peaks appear due to migration of protons from the terminal and bridging sites of **14b** to **14a**, but no cross-peaks appear corresponding to terminal/bridge exchange in **14b** at −35 °C. As a consequence, any independent bridge/terminal hydride exchange in **14b** has a higher barrier than equilibration of **14a** with **14b**.

Each of the two structures of $[(silox)_2TaH]_2(\mu\text{-}H)_2(\mu\text{-}O)$, **14a** and **14b**, possesses inequivalent silox groups, equivalent terminal hydrides, and equivalent bridging hydrides. The equilibrium between them, defined as **14a** $\rightleftharpoons$ **14b** (K_{eq} = [**14b**]/[**14a**]), was mildly temperature dependent (^1H NMR measurements); a plot of ln K_{eq} vs $1/T$ between −50 and −15 °C yielded a ΔH of −1.1(3) kcal/mol and a ΔS of −5(1) eu. The spectral similarities of the two isomers and the minimal differences in their free energies suggest that they differ only in the rotational arrangement of the ligands about the tantalum center, as Figure 1 depicts. Isomer **14a** has been tentatively assigned a C_2 face-shared bioctahedral geometry, and **14b** is illustrated as a C_2 bitrigonal prism, with the common faces of both comprising the μ-oxo and μ-hydrides. The assignment of these configurations is somewhat arbitrary, since the NMR data cannot distinguish between them, and attempts to obtain single crystals proved fruitless. Compound **14** reproducibly crystallizes as a bundle of fibers, characterized by rotation photographs indicating only one unique axis. Sterically, the two configurations are nearly identical, according to molecular models.

Several mechanisms can be used to rationalize the dynamic behavior of **14**. The dashed arrows in Figure 1 illustrate the possibility of exchange via an intermediate structure **14**-I, that contains equivalent hydride and silox ligands. The configuration of **14**-I is attractive because its staggered D_{2d} symmetry and axial hydrides are reminiscent of $[(silox)_2TaH_2]_2$ (**11**), and the trigonal oxygen coordination geometry is analogous to that of $(silox)_3TaH_2$ (**2**). In fact, the bioctahedral geometry is assigned to **14a**, because if its hydride bridges are broken, only a slight distortion is required to generate **14**-I. More rearrangement is needed to form **14**-I from **14b**; hence, the structural assignments have been based on this particular mechanistic bias.

The variable-temperature NMR spectroscopy data does not require an intermediate to be present. The only stipulation is the requirement that the fluxionality of **14b** occur via **14a**; hence, no

(46) (a) Parkin, G.; van Asselt, A.; Leahy, D. J.; Whinnery, L.; Hua, N. G.; Wuan, R. W.; Henling, L. M.; Schaefer, W. P.; Santarsiero, B. D.; Bercaw, J. E. *Inorg. Chem.* **1992**, *31*, 82–85. (b) Parkin, G.; Bercaw, J. E. *J. Am. Chem. Soc.* **1989**, *111*, 391–393.

(47) Nugent, W. A.; Mayer, J. M. *Metal-Ligand Multiple Bonds*; Wiley-Interscience: New York, 1988.

(48) Carpenter, B. K. *Determination of Organic Reaction Mechanisms*; John Wiley and Sons: New York, 1984. Due to zero-point energy differences, deuterium will prefer strongly bound terminal over bridging sites.

(49) For a similar experiment, see: Cotton, F. A.; Luck, R. L.; Root, D. R.; Walton, R. A. *Inorg. Chem.* **1990**, *29*, 43–47.

(50) For binuclear hydrides with terminal sites upfield of bridging, see: (a) Fryzuk, M. D.; McConville, D. H. *Inorg. Chem.* **1989**, *28*, 1613–1614. (b) Green, M. A.; Huffman, J. C.; Caulton, K. G. *J. Am. Chem. Soc.* **1982**, *104*, 2319–2320. (c) Green, M. A.; Huffman, J. C.; Caulton, K. G. *Ibid.* **1981**, *103*, 695–696.

(51) Derome, A. E. *Modern NMR Techniques for Chemistry Research*; Pergamon: Oxford, 1987.

(52) (a) Meier, B. H.; Ernst, R. R. *J. Am. Chem. Soc.* **1979**, *101*, 6441–644242. (b) Jeener, J.; Meier, B. H.; Bachmann, P.; Ernst, R. R. *J. Chem. Phys.* **1979**, *71*, 4546–4553.

(53) At long τ_m (200 ms), off-diagonal peaks corresponding to **14b** terminal–bridge transfer appear; these are interpreted as second-order peaks arising from multiple exchange events. In principle, the experiment also records NOE transfer. However, since the rate of buildup of NOE is at most $1/T_1$, choosing $\tau_m \approx 0.01(T_1)$ effectively eliminates NOE contributions.

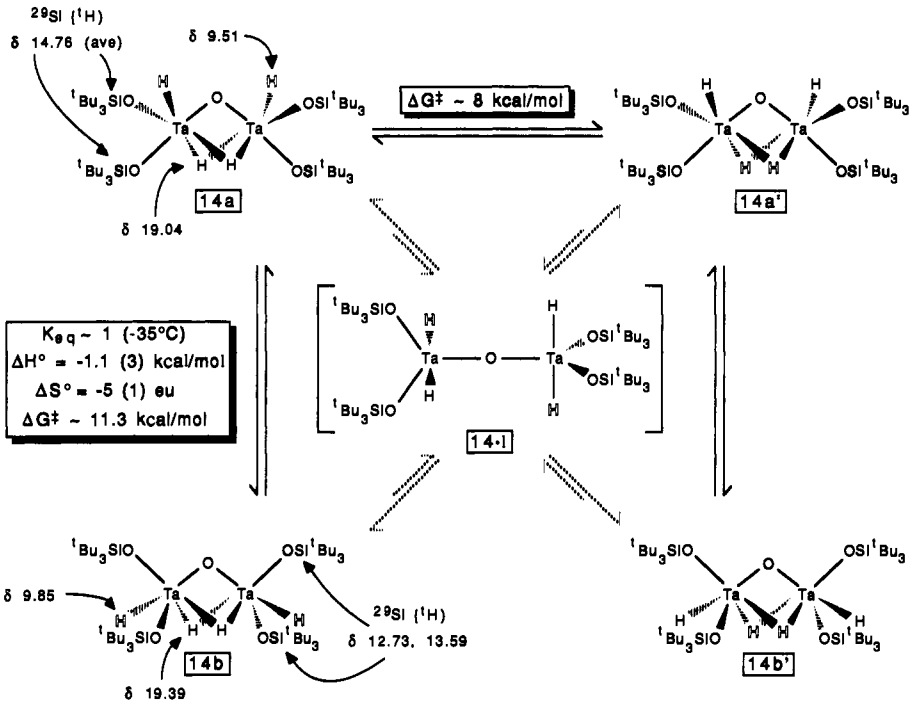

Figure 1. Pathways and energetics for interchange of **14a** and **14b**, conformational isomers of $[(silox)_2TaH]_2(\mu\text{-}H)_2(\mu\text{-}O)$, as determined from variable-temperature ^1H and $^{29}Si\{^1H\}$ NMR.

direct H_t/H_b exchange for **14b** is shown by the solid arrows in Figure 1. A turnstile rotation of the $(silox)_2HTa$ centers may be responsible for the interconversion of **14a** with **14b**, while various exchange pathways may be implicated to describe the terminal/bridging hydride fluxionality of **14a**. Virtually any pathway will also exchange silox groups in concert with the hydrides.

Molecular Structure of $[(silox)_2TaH_2]_2$ (11). The single-crystal X-ray structure determination of $[(silox)_2TaH_2]_2$ (**11**) confirmed its D_{2d} geometry, as illustrated in the molecular and skeletal views of Figure 2. The dimer crystallized in a cubic space group ($I\bar{4}3d$, 1190 reflections ($F > 3.0\sigma(F)$), $R = 7.9\%$, $R_w = 5.0\%$) with each molecule possessing $\bar{4}$ symmetry along the Ta–Ta vector. The asymmetric unit comprised $TaHOSi^tBu_3$ with the Ta atom residing on a 2-fold axis. Due to the high symmetry and relatively limited data, isotropic refinement of the carbons was required, but the remaining atoms were refined anisotropically. As a consequence, the geometry of the peripheral ^{t}Bu groups is relatively poor, although their average distances and angles are normal, and the hydride positions have not been determined.

Despite these concerns, the $Ta_2O_4Si_4$ core is well defined. The equatorial oxygens and the metal–metal bond lie in a near-perfect trigonal plane ($\angle$Ta–Ta–O = 120.7(8)°, $\angle$O–Ta–O = 118.7(11)°), and the Ta–O–Si angle is nearly linear (174.7(20)°), as expected.[9,54] The Ta–Ta single bond distance is 2.720(4) Å, a value proximate to the sum of tantalum covalent radii (2.68 Å).[55] Given the IR evidence and the crystallographic symmetry, the hydrides must be terminal, residing above and below the $TaO_2(Ta)$ trigonal planes. Alternate structures involving $Ta_2(\mu\text{-}H)_4$ or $(TaH)_2(\mu\text{-}H)_2$ bridges are spectroscopically and crystallographically untenable. The absence of bridging hydrides is surprising in view of their propensity to bridge in early metal systems. It is tempting to conclude that μ-H ligands would compete ineffectively for orbitals used in $O(p\pi) \rightarrow Ta(d\pi)$ donation, but the Ta–O distance is normal (1.86(3) Å) as is the Si–O (1.70(3) Å) bond length;[9,54] therefore, it is unlikely that the silox ligands of **11** are donating substantially greater electron density than has previously been observed. In addition, bridging hydrides are clearly present in $[(silox)_2TaH]_2(\mu\text{-}H)_2(\mu\text{-}O)$ (**14**), a complex with additional oxygen π-donation. The pronounced steric influence of the intermeshed silox groups probably enforces the highly symmetric D_{2d} structure of **11**, in turn dictating the unusual terminal disposition of the hydrides.

H/D Exchange Processes of Hydrides. 1. Isotopomers of $[(silox)_2TaH]_2$ (11). When $(silox)_2TaCl_3$ (**9**) was reduced in the presence of a 1:1 mixture of H_2 and D_2, the ^1H NMR spectrum of the $(silox)_4Ta_2D_nH_{4-n}$ (**11**-d_n) product revealed resonances of four proton-containing isotopomers that integrated (~1:3:3:1) according to the predicted statistical ratio, 1:4:6:4 (**11**:**11**-d_1:**11**-d_2:**11**-d_3). Figure 3 shows that the signals corresponding to **11**-d_1, **11**-d_2, and **11**-d_3 were shifted ~0.02, 0.04, and 0.06 ppm *downfield* from tetrahydride **11**. While the magnitude of the NMR isotope shift is typical for *gem*-substitution, downfield shifts are extremely rare.[56,58] In contrast, the hydride of $(silox)_3TaHD$ (**2**-d_1), prepared in a statistical mixture (2:1:1) with **2** and **2**-d_2 from reduction of $(silox)_3TaCl_2$ (**1**) under HD, resonates 0.02 ppm upfield of the dihydride (**2**). The additive effect of deuterium substitution (+0.022 ppm per D at 23 °C) and the appearance of a single peak for the two possible isomers of D_{2d} **11**-d_2 (i.e.,

(54) (a) Neithamer, D. R.; Párkányi, L.; Mitchell, J. F.; Wolczanski, P. T. *J. Am. Chem. Soc.* **1988**, *110*, 4421–4423. (b) Eppley, D. F.; Wolczanski, P. T.; Van Duyne, G. D. *Angew. Chem., Int. Ed. Engl.* **1991**, *30*, 584–585.

(55) Messerle, L. *Chem. Rev.* **1988**, *88*, 1229–1254.

(56) (a) Hanson, P. E. *Annu. Rep. NMR Spectrosc.* **1983**, *15*, 105–234. (b) Jameson, C. J. *J. Chem. Phys.* **1977**, *66*, 4983–4988. (c) Batiz-Hernandez, H.; Bernheim, R. A. *Prog. Nucl. Magn. Reson. Spectrosc.* **1967**, *3*, 63–85. For an interesting example of a downfield isotope shift in certain benzyl phosphonates, see: Lee, S.-G.; Bentrude, W. G. *Phosphorus Sulfur* **1988**, *35*, 219–222.

(57) A downfield shift is observed in $OsD_nH_{4-n}\{P(tol\text{-}d_2)_3\}_3$. See: Desrosiers, P. J.; Cai, L.; Lin, Z.; Richards, R.; Halpern, J. *J. Am. Chem. Soc.* **1991**, *113*, 4173–4184.

(58) An alternative explanation[59] of the downfield shifts relies on the existence of an energetically accessible isomer such as $[(silox)_2TaH]_2(\mu\text{-}H)_2$ (**11'**), containing chemically and magnetically distinct hydride sites. The downfield shift could reflect an equilibrium overpopulation of ^1H in bridging (downfield) sites of **11'** due to the preference of D for the more strongly bound terminal position. Rapid **11** ⇌ **11'** exchange produces an averaged ^1H NMR signal shifted downfield according to the degree of deuteration of the molecule. The downfield shift reported for $OsD_nH_{4-n}\{P(tol\text{-}d_2)_3\}_3$[57] could be similarly created by rapid equilibration with a dihydrogen complex, $OsH_2(H_2)\{P(tol\text{-}d_2)_3\}_3$. Such effects would be relatively subtle, yet the magnitudes of the shifts observed for both complexes imply a *substantial* population of the higher lying species and/or a large chemical shift difference between the sites. In neither case has independent spectroscopic evidence for a low-lying isomer been detected. Halpern, J. Private communication.

(59) For further discussion of isotopomers and H/D exchange processes of **11**, see: Miller, R. L. Ph.D. Thesis, Cornell University, Ithaca, NY, 1993.

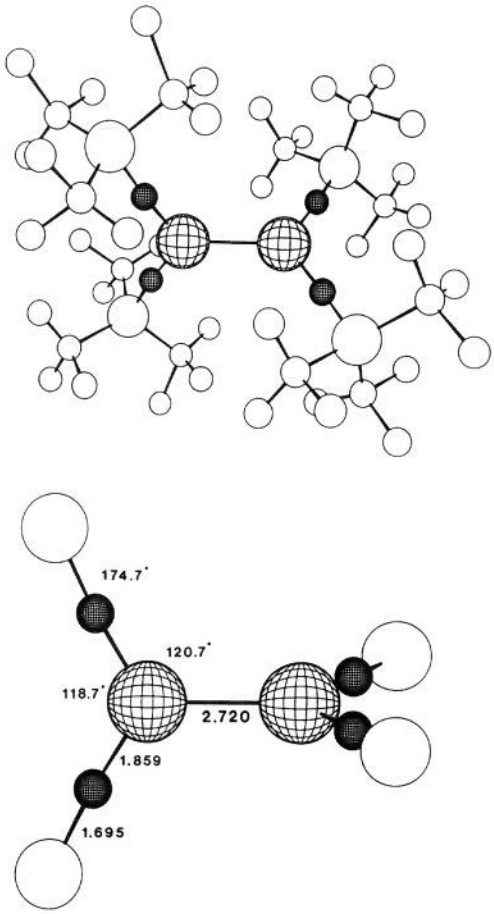

Figure 2. Molecular structure and skeletal view of $[(silox)_2TaH_2]_2$ (**11**). Bond distances (angstroms): Ta–Ta, 2.720(4); Ta–O, 1.859(24); Si–O, 11.695(28); Si–C(av), 2.02(2); C–C(av), 1.52(14). Bond angles (degrees): Ta–Ta–O, 120.7(8); O–Ta–O, 118.7(11); Ta–O–Si, 174.7(20); O–Si–C(av), 102.1(44); Si–C–C(av), 107.8(27); C–C–C(av), 110.7(89).

11-*1,1*-d_2 and **11**-*1,2*-d_2) require the three-bond perturbation to be coincidentally equal to the two-bond effect, contrary to the expected decrease in isotope shift with increasing distance from the heavy atom.[56] Alternatively, the additive effect may reflect a rapid fluxionality in **11**-d_n, where the perturbation is an average of the two- and three-bond components in each isotopomer.[60] The fluxionality could occur via a transition state or intermediate containing bridging hydrides, such as $[(silox)_2TaH]_2(\mu\text{-H})_2$ or $[(silox)_2Ta]_2(\mu\text{-H})_4$.

2. Dihydrogen Exchange with $(silox)_3TaH_2$ (2) and 11. When $(silox)_3TaH_2$ (**2**) was exposed to D_2 in benzene-d_6 at 25 °C, rapid H/D exchange (<5 min) occurred to provide $(silox)_3TaHD$ (**2**-d_1, δ 21.97) and $(silox)_3TaD_2$ (**2**-d_2). Since hydrido deuteride **2**-d_1 was produced, it is unlikely that reductive elimination of H_2 from **2** is responsible. A non-pairwise, σ-bond metathesis pathway is more consistent with the labeling result and the rate of exchange.

The hypothetical Ta(V) species, $(silox)_2TaH_3$, was sought as an analogue of known bis-cyclopentadienyl trihydrides.[61] However, dinuclear oxidative addition of H_2 to $[(silox)_2TaH_2]_2$ (**11**) proved unfavorable: the ^{1}H NMR spectrum of **11** and H_2 (55.1 atm) showed no new species, and only the dimeric tetrahydride was recovered upon exposure of **11** to 100 atm of H_2 at 100 °C (12 h). Nonetheless, hydrocarbon solutions of **11** rapidly incorporated deuterium when exposed to D_2, providing a convenient synthesis of $[(silox)_2TaD_2]_2$ (**11**-d_4). Evolved H_2 and HD were repeatedly purged from the system in order to complete the deuteration. Attempts to monitor the appearance of isotopomers **11**-d_n during the reaction using routine kinetics methods (^{1}H NMR) were hampered because equilibration with dissolved D_2 occurred before a spectrum could be acquired. After the initial fast equilibration, the observed exchange rate slowed measurably, appearently due to slow diffusion of D_2 across the gas–solution interface. By agitating the tube, additional D_2 was admitted to the solution and exchange proceeded swiftly.

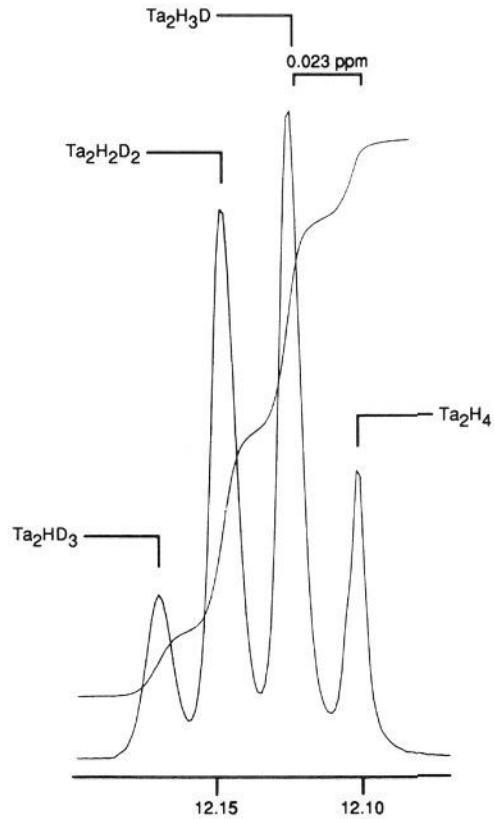

Figure 3. Hydride resonances in the ^{1}H NMR spectrum of $(silox)_4Ta_2D_nH_{4-n}$ (**11**-d_n) showing an NMR isotope effect of 0.023 ppm at 23 °C. Resonances for **11**-d_3, **11**-d_2, **11**-d_1, and **11** integrated ~1:3:3:1 according to the predicted statistical ratio for **11**-d_4:**11**-d_3:**11**-d_2:**11**-d_1:**11** of 1:4:6:4:1.

Magnetization transfer experiments (^{1}H NMR)[51] determined the rate of dihydrogen exchange with **11**.[62] Toluene-d_8 solutions of the tetrahydride (**11**) were sealed in single-crystal sapphire NMR tubes under dihydrogen pressures of 14.3 and 55.1 atm, and solution H_2 concentrations were measured directly by integrated intensity in the temperature range 10–110 °C. A

$$\underset{\mathbf{11}}{[(silox)_2TaH_2]_2} + H^*_2 \xrightarrow{k} (silox)_4Ta_2H_3H^* + HH^* \qquad (2)$$

rapid second-order exchange of H_2 with **11** was observed (eq 2), as the data in Table III indicate (e.g., 50 °C, $k = 9.2(3) \times 10^2$ M^{-1} s^{-1}; 100 °C, $k = 3.3(2) \times 10^3$ M^{-1} s^{-1}; $\Delta H^{\ddagger} = 6.2(1)$ kcal/mol, $\Delta S^{\ddagger} = -26(3)$ eu). Magnetization transfer from the hydrides of **11** to dihydrogen was also measured, and the exchange rate constant paralleled that of eq 2. The activation parameters support

(60) Define $\Delta\delta_2$ as the two-bond perturbation and $\Delta\delta_3$ as the three-bond perturbation. The perturbation would then be $(\Delta\delta_2 + 2\Delta\delta_3)/3$ for **11**-d_1 and $(\Delta\delta_2 + 2\Delta\delta_3)$ for **11**-d_3. The perturbation on **11**-d_2 would be a statistical (1:2) average of that for $(silox)_2H_2Ta_2D_2(silox)_2$ $(2\Delta\delta_3)$ and $[(silox)_2TaHD]_2$ $(\Delta\delta_2 + \Delta\delta_3)$, which amounts to $2/3(\Delta\delta_2 + 2\Delta\delta_3)$.

(61) (a) Green, M. L. H.; McCleverty, J. A.; Pratt, L.; Wilkinson, G. *J. Chem. Soc.* **1961**, 4854–4859. (b) Gibson, V. C.; Bercaw, J. E.; Bruton, W. J., Jr.; Sanner, R. D. *Organometallics* **1986**, *5*, 976–979.

(62) (a) Roe, D. C. *Organometallics* **1987**, *6*, 942–946. (b) Roe, D. C. *J. Magn. Reson.* **1985**, *63*, 388–391.

Table III. Second-Order Rate Constants for Exchange between $[(silox)_2TaH_2]_2$ (**11**) and Dihydrogen Obtained from Magnetization Transfer Experiments[a,b]

	14.3 atm of H_2		55 atm of H_2	
T (°C)	$[H_2]$ (M)	k ($\times 10^{-2}$ M^{-1} s^{-1})	$[H_2]$ (M)	k ($\times 10^{-2}$ M^{-1} s^{-1})
10			0.146	2.5
20			0.158	3.3
30			0.171	5.1
40	0.059	6.9	0.185	6.7
50	0.057	9.2	0.202	8.7
60	0.061	11.8	0.218	11.5
70	0.060	15.7	0.235	14.7
80	0.067	20.5	0.253	19.5
90	0.068	25.2	0.272	27.3
100	0.072	34.0	0.282	33.0
110	0.078	45.9	0.306	44.1
120	0.078	56.9		

[a] Data were taken from transfer of magnetization from **11** to H_2, corrected for statistics, and checked by measuring transfer from H_2 to **11**. [b] From an Eyring plot: $\Delta H^{\ddagger} = 6.2(1)$ kcal/mol, $\Delta S^{\ddagger} = -26(3)$ eu (cal/mol·K).

a σ-bond metathesis pathway and are comparable to related exchanges involving the extremely electrophilic metal center in Cp^*_2ScR.[63]

When **11** and **11**-d_4 were mixed in hydrocarbon solvents, a statistical distribution of isotopomers **11**-d_n (n = 0–4) gradually formed. ^{1}H NMR monitoring revealed preferential formation of **11**-d_1 and **11**-d_3 at early stages of the reaction. While the experimental curves appeared well-behaved, rate constants k_{obsd} for the decay of **11**-d_0 to its statistical concentration[64] varied sporadically between $\sim 10^{-3}$ and 10^{-4} s^{-1} with no evident dependence upon [**11**-d_n]. Extensive experimentation[59] tentatively suggested that the exchange proceeds via σ-bond metathesis catalyzed by traces of H_2/D_2.[65]

Carbonylation Studies. 1. Monomeric Hydrides. Exposure of $(silox)_3TaHR$ (R = H, **2**; Et, **5**) to CO at 25 °C afforded monomeric formaldehyde, $(silox)_3Ta(\eta^2\text{-}OCH_2)$ (**15**),[66,67] and propanal, $(silox)_3Ta(\eta^2\text{-}OCHEt)$ (**16**), complexes[68,69] in 77% and 41% isolated yields upon crystallization from Et_2O (eq 3).

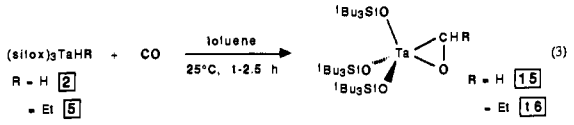

According to sealed NMR tube experiments, $(silox)_3Ta(\eta^2\text{-}OCH_2)$ (**15**) was formed immediately in essentially quantitative yield (>98% by ^{1}H NMR) under 2 atm of CO, and no subsequent insertion product was evidenced, even when the tube was heated at 120 °C. Both species are colorless, indicating that a Ta(V) metallaepoxide depiction is most appropriate. In a sealed NMR tube, the exposure of $(silox)_3Ta$ (**3**) to excess paraformaldehyde in C_6D_6 at 64 °C for 20 min was shown to effect the formation of **15** (eq 4). Similarly, addition of propanal to **3** generated $(silox)_3Ta(\eta^2\text{-}OCHEt)$ (**16**) in 63% isolated yield (eq 5). Adduct formation was extremely clean (^{1}H NMR); hence, the high solubility of **16** was responsible for the mediocre yields.

$$(silox)_3Ta\ (\mathbf{3}) + (CH_2O)_n\ (\text{excess}) \xrightarrow[64\ °C,\ 20\ min]{C_6D_6} (silox)_3Ta(\eta^2\text{-}OCH_2)\ (\mathbf{15}) \quad (4)$$

$$3 + EtCHO \xrightarrow[30\ min,\ 25\ °C]{hexanes} (silox)_3Ta(\eta^2\text{-}OHCEt)\ (\mathbf{16}) \quad (5)$$

^{13}C chemical shifts of the aldehydic carbons corresponding to **15** (δ 93.87, J_{CH} = 159 Hz) and **16** (δ 111.67, J_{CH} = 152 Hz) are more consistent with the CHR ($\delta \sim 60$) and methylene ($\delta \sim 45$) resonances of substituted epoxides ($HRCCH_2O$) than those of aldehydes ($\delta \sim 200$). The carbon–hydrogen coupling constants are ambiguous, falling in a region somewhat smaller than do organic epoxides or aldehydes.[70] ^{1}H chemical shifts of the CHR (**15**, CH_2, δ 4.06; **16**, C*H*Et, δ 4.46) fragments are also near those of organic ethers ($\delta \sim 3$–4) and epoxides ($\delta \sim 2$–3) and clearly support the metallaepoxide depiction. NMR spectra (Table IV) of each aldehyde adduct revealed one type of silox, reflecting a low barrier to rotation of the η^2-OCHR ligand on the cylindrically symmetric C_{3v} $(silox)_3Ta$ fragment.[37] From the IR spectra of **15** and **15**-^{13}C, prepared from **2** and ^{13}CO, a ν(CO) of 932 cm^{-1} was identified by its shift to 914 cm^{-1} upon isotopic labeling, again consistent with the metallaepoxide description.

When a 1:1 mixture of $(silox)_3TaH_2$ (**2**) and **2**-d_2 in benzene-d_6 was exposed to CO at pressures greater than 5 atm, $(silox)_3Ta(\eta^2\text{-}OCH_2)$ (**15**) and $(silox)_3Ta(\eta^2\text{-}OCD_2)$ (**15**-d_2) were the sole products (>98%), indicative of intramolecular CO reduction (eq 6). Curiously, at lower pressures, some crossover

$$(silox)_3TaH_2\ (\mathbf{2}) + (silox)_3TaD_2\ (\mathbf{2}\text{-}d_2) \xrightarrow[CO\ (>5\ atm),\ 25\ °C]{C_6D_6,\ <15\ min} (silox)_3Ta(\eta^2\text{-}OCH_2)\ (\mathbf{15}) + (silox)_3Ta(\eta^2\text{-}OCD_2)\ (\mathbf{15}\text{-}d_2) \quad (6)$$

was evident. The same mixture of **2** and **2**-d_2, when exposed to 2 equiv of CO, generated $\sim$15% $(silox)_3Ta(\eta^2\text{-}OCHD)$ (**15**-d_1; ^{1}H NMR δ 4.03). This crossover product was initially attributed to a competitive intermolecular reduction pathway,[29] since neither **2** and **2**-d_2 nor **15** and **15**-d_2 were found to exchange under similar conditions. However, an intermolecular process, disfavored from kinetic (i.e., second-order dependence on metal) and steric standpoints, appears less likely in view of the rapid dihydrogen exchange reactions of **2**. Generation of traces of H_2/D_2 by exposure of **2** and **2**-d_2 to CO in a sealed NMR tube could easily account for the "crossover" product, rendering the control experiment moot. Unfortunately, the carbonylation reaction is too fast, even at low [CO], to monitor the appearance of **2**-d_1 at low conversion; thus, the formation of the η^2-formaldehyde derivative is presumed to occur intramolecularly under all conditions. Generation of **15** is believed to be the only discrete, mononuclear CO to formaldehyde transformation known, al-

(63) (a) Thompson, M. E.; Baxter, S. M.; Bulls, A. R.; Burger, B. J.; Nolan, M. C.; Santarsiero, B. D.; Schaefer, W. P.; Bercaw, J. E. *J. Am. Chem. Soc.* **1987**, *109*, 203–219. (b) Thompson, M. E.; Bercaw, J. E. *Pure Appl. Chem.* **1984**, *56*, 1–11.

(64) Espenson, J. H. *Chemical Kinetics and Reaction Mechanisms*; McGraw-Hill: New York, 1981.

(65) One plausible, somewhat spurious source of H_2/D_2 is trace hydrolysis of **11**/**11**-d_4 incurred from miniscule amounts of H_2O liberated through flame-sealing of NMR tubes, which are flame-dried prior to loading.

(66) For representative mononuclear formaldehyde complexes, see: (a) Herberich, G. E.; Okuda, J. *Angew. Chem., Int. Ed. Engl.* **1985**, *24*, 402. (b) Green, M. L. H.; Parkin, G. *J. Chem. Soc., Chem. Commun.* **1986**, 90–91. (c) Green, M. L. H.; Parkin, G.; Moynihan, K. J.; Prout, K. *Ibid.* **1984**, 1540.

(67) van Asselt, A.; Burger, B. J.; Gibson, V. C.; Bercaw, J. E. *J. Am. Chem. Soc.* **1986**, *108*, 5347–5349. Conversion of $Cp^*_2TaH(\eta^2\text{-}CH_2O)$ ($Cp^* = \eta^5\text{-}C_5Me_5$) to $Cp^*_2Ta{=}O(CH_3)$ must involve a pathway related to **20** to **21**, including a CO oxidative addition after formation of transient $Cp^*_2Ta(OCH_3)$.

(68) For η^2-aldehydes, see: (a) Roddick, D. M.; Bercaw, J. E. *Chem. Ber.* **1989**, *122*, 1559–1578. (b) Hofmann, P.; Stauffert, P.; Frede, M.; Tatsumi, K. *Ibid.* **1989**, *122*, 1579–1587 and references cited therein.

(69) (a) Tatsumi, K.; Nakamura, A.; Hofmann, P.; Stauffert, P.; Hoffmann, R. *J. Am. Chem. Soc.* **1985**, *107*, 4440–4451. (b) Hofmann, P.; Stauffert, P.; Tatsumi, K.; Nakamura, A.; Hoffmann, R. *Organometallics* **1985**, *3*, 404–406. (c) Tatsumi, K.; Nakamura, A.; Hofmann, P.; Hoffmann, R.; Moloy, K. G.; Marks, T. J. *J. Am. Chem. Soc.* **1986**, *108*, 4467–4476 and references cited therein.

(70) (a) Marshall, J. L. *Carbon-Carbon and Carbon-Proton NMR Couplings*; Verlag Chemie International: Deerfield Beach, FL, 1983. (b) Leydon, D. E.; Cox, R. H. *Analytical Applications of NMR*; John Wiley & Sons: New York, 1977.

Table IV. NMR (δ in ppm (m, J in Hz))[a] Data for Carbonylation Products of $(silox)_3TaHR$ (R = H, **2**; Et, **5**), $[(silox)_2TaH_2]_2$ (**11**), $[(silox)_2TaH]_2(\mu\text{-}O)_2$ (**12**), and $[(silox)_2HTa]_2(\mu\text{-}H)_2(\mu\text{-}O)$ (**14**)

	^1H[b]		$^{13}C\{^1H\}$ or ^{13}C[c]	
compound	silox	other	$Si(C(CH_3)_3)_3$[d]	other[e]
$(silox)_3Ta(\eta^2\text{-}OCH_2)$ (**15**)	1.25	4.06	23.56, 30.58	93.87 (CH_2, 159)
$(silox)_3Ta(\eta^2\text{-}OCHEt)$ (**17**)	1.27	1.35 (Me, t, 7.1)	23.57, 30.61	17.15 (CH_3, 126)
		2.22 (C*H*H, ddq; 9.6, 14, 7.1)		111.67 (CHEt, 152)
		2.27 (CH*H*, ddq; 3.3, 14, 7.1)		
		4.46 (CHEt, dd; 3.3, 9.6)		
$[(silox)_2TaCl]_2(\mu\text{-}H)(\mu\text{:}\eta^2,\eta^2\text{-}CHO)$ (**18**)	1.24	6.18 (CHO, d, 2.8)	23.76, 30.39	160.3 (CHO, 167, 3)
	1.26	9.56 (TaH, d, 2.8)	24.00	
	1.28		24.32	
	1.36		25.76	
$[(silox)_2TaH]_2(\mu\text{-}CH_2)(\mu\text{-}O)$ (**19**)	1.28	7.08 (CH_2)	23.56, 30.56	178.10 (CH_2, 135)
		15.99 (TaH)		
$[(silox)_2TaH](\mu\text{:}\eta^2,\eta^2\text{-}CHO)$	1.15	2.92 (C*H*HO, d, 3.5)	23.49, 30.52	79.08 (CH_2O, 159)
$(\mu\text{:}\eta^1,\eta^2\text{-}CH_2O)[Ta(silox)_2]$ (**20**)	1.21	3.36 (CH*H*O, d, 3.5)	23.64, 30.60	134.94 (CHO, 166)
	1.30	5.80 (CHO)	23.84, 30.86	
	1.35	14.99 (TaH)	24.07, 31.17	
$[(silox)_2Ta]_2(\mu\text{-}O)_2(\mu\text{-}CHMe)$ (**21**)	1.28	3.81 ($CHCH_3$, d, 7.4)	23.97, 30.53	25.67 (128, 4, 36*)
		5.51 (CHMe, q, 7.4)		191.22 (109, 7, 36*)
$[(silox)_2Ta]_2(\mu\text{:}\eta^1,\eta^1\text{-}CH{=}CHO)$	1.26 (2)	3.79 (C*H*HO, d, 2.9)	23.76, 30.28	89.32 (CH_2O, 158)
$(\mu\text{:}\eta^1,\eta^2\text{-}CH_2O)(\mu\text{-}O)$ (**22**)	1.29	3.97 (CH*H*O, d, 2.9)	23.78 (2), 30.50	162.40 (OCH=, 181, 62*)
	1.33	7.04 (=CHTa, d, 7.5)	23.82, 30.63	167.18 (=CHTa, 141, 9, 62*)
		8.43 (OCH=, d, 7.5)	30.70	
$[(silox)_2Ta]_2(\mu\text{-}O)_2(\mu\text{-}CH_2O)$ (**23**)	1.17 (2)	4.33 (CH_2)	23.45 (2), 29.91	96.64 (CH_2O, 160)
	1.35		23.99, 30.58	
	1.36		24.05	
$[(silox)_2HTa]_2(\mu\text{-}O)_2[TaMe(silox)_2]$ (**24**)	1.28	1.52 (TaMe)	23.40, 30.28	50.6 (Me, 123)
	1.29 (br)	20.67 (TaH)	23.54, 30.42 (3)	
			23.97 (2)	
$[(silox)_2Ta]_2(\mu\text{-}O)_2(\mu\text{:}\eta^2,\eta^1\text{-}MeCHO)$ (**25**)	1.14	2.43 ($CHCH_3$, d, 6.3)	23.71–24.27 (4)	21.71 ($CHCH_3$, 126, 38*)
	1.18	5.04 (CHMe, q, 6.2)	30.44, 30.57	110.11 (CHMe, 157, 38*)
	1.38		30.83, 30.92	
	1.42			

[a] Benzene-d_6 unless otherwise noted. [b] Referenced to Me_4Si at δ 0.0 or benzene-d_6 at δ 7.15. [c] Referenced to benzene-d_6 at δ 128.00 [d] Listed as SiC, $C(CH_3)_3$; the $^1J_{CH}$ for the silox methyls is typically 123–126 Hz. [e] Couplings are given in the order $^1J_{CH}$, $^nJ_{CH}$, $^1J_{CC}$(*).

though Erker's preparation of trimeric $[Cp_2Zr(\mu\text{:}\eta^2,\eta^1\text{-}OCH_2)]_3$ by carbonylation of $[Cp_2ZrH_2]_n$ may occur similarly.[71,72]

Carbonylation of $(silox)_3TaH_2$ (**2**) is expected to proceed stepwise via a transient, thermodynamically accessible formyl, $(silox)_3HTa(\eta^2\text{-}CHO)$ (**17**). Subsequent formyl hydride reductive elimination, or hydride to η^2-CHO transfer,[23,68,69,71-73] would result in $(silox)_3Ta(\eta^2\text{-}OCH_2)$ (**15**). Since **17** was not detected, carbonylations of the $(silox)_3HTaX$ derivatives were undertaken in the hope of observing formyl species.[74] Exposure of $(silox)_3HTaX$ (X = Cl, **6**-Cl; I, **6**-I) to excess CO and subsequent thermolysis (~80 °C) failed to provide evidence of formyls, but disproportionation products were noted when the solutions were photolyzed. Hydrochloride **6**-Cl generated $(silox)_3TaCl_2$ (**1**) and **15**, presumably formed from dihydride **2**, and a similar result was obtained with photosensitive **6**-I. The additional π-donor ligand (e.g., Cl, I) may render a formyl less thermodynamically accessible by competing with η^2-coordination by the HCO unit.

2. Dimeric Hydrides. In examining the carbonylation chemistry of the dimeric hydrides, yields and purity of the derivatives varied greatly depending on the experimental conditions. This discussion focuses on conditions that maximized the purity of the complexes, since thermal stability was a significant problem for several. While the majority of the carbonylations occurred immediately at 25 °C, according to ^1H NMR tube experiments, serendipity played an important role in their isolation. Certain thermally sensitive carbonylation products precipitated from solution faster than they reacted with CO, permitting low-temperature isolation and subsequent spectral characterization (Table IV). Quenching procedures were also varied to obtain the most reproducible yields of organic products.

Treatment of $[(silox)_2TaCl]_2(\mu\text{-}H)_2$ (**10**) with excess CO yielded $[(silox)_2TaCl]_2(\mu\text{-}H)(\mu\text{:}\eta^2,\eta^2\text{-}CHO)$ (**18**, 56%) as a light yellow powder (~90–95% pure) upon precipitation from Et_2O at –78 °C (eq 7). The formyl hydride was thermally sensitive

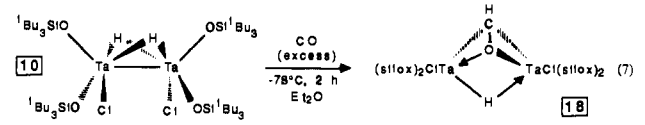

($t_{1/2}$(decomposition) ≈ 3 h in benzene, $t_{1/2}$ ≈ 12 h in the solid state), decomposing to uncharacterized products at room temperature, but it could be kept for significant periods of time at –20 °C. When subjected to 3 equiv of HCl (g), **18** generated 0.87 equiv of dihydrogen, consistent with the presence of a hydride. Hydrolysis of **18** produced 0.86 equiv of CH_3OH, presumably via electrophilic cleavage of the formyl functionality.

The hydride assignment was borne out by the ^1H NMR spectrum of **18**, which contained a resonance at δ 9.56 coupled to the formyl at δ 6.18 (J_{HH} = 2.8 Hz). ^{13}C NMR spectra of **18**-^{13}C, prepared from **10** and ^{13}CO, revealed a somewhat broad resonance for the formyl at δ 160.3 with a J_{CH} of 167 Hz and a small coupling ($^3J_{CH}$ = 3 Hz) to the hydride. The IR spectrum exhibited a very broad $\nu(Ta_2H)$ at 1270 cm^{-1}, consistent with a bridging hydride. The spectral parameters are notably similar to Schrock's structurally characterized $[(\eta^5\text{-}C_5Me_4Et)TaCl_2]_2(\mu\text{-}H)(\mu\text{:}\eta^2,\eta^2\text{-}CHO)$ complex (^1H NMR δ 5.6 (TaH), 7.5 (OCH); ^{13}C NMR δ 168 (OCH); J_{HH} = 4 Hz, J_{CH} = 168 Hz, $^3J_{CH}$ = 20 Hz; IR $\nu(Ta_2H)$ 1288 cm^{-1}),[33] which displayed an inequivalence of its tantalum centers. Similarly, **18** possesses inequivalent silox groups on distinct tantalums, revealed by four independent

(71) Kropp, K.; Skibbe, V.; Erker, G.; Krüger, C. *J. Am. Chem. Soc.* **1983**, *105*, 3353–3354.
(72) (a) Erker, G.; Hoffmann, U.; Zwettler, R.; Betz, P.; Krüger, C. *Angew. Chem., Int. Ed. Engl.* **1989**, *28*, 630–631. (b) Curtis, C. J.; Haltiwanger, R. C. *Organometallics* **1991**, *10*, 3220–3226.
(73) Wolczanski, P. T.; Bercaw, J. E. *Acc. Chem. Res.* **1980**, *13*, 121–127.
(74) Moloy, K. G.; Marks, T. J. *J. Am. Chem. Soc.* **1984**, *106*, 7051–7064 and references cited therein. A pertinent discussion regarding kinetic and thermodynamic aspects of Th–H vs Th–CH_3 carbonylations is included.

Scheme III

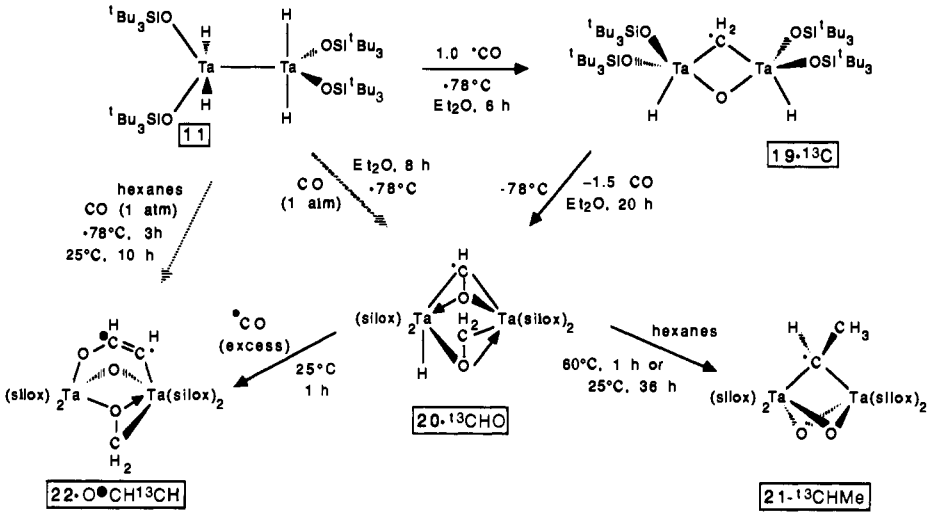

resonances in the ^1H and ^{13}C NMR (SiC) spectra. This spectral signature is a consequence of the asymmetric bridges of **18** and the diastereotopic silox ligands of each $(silox)_2ClTa$ fragment.

Scheme III illustrates an interrelated series of carbonylations starting from the tetrahydride complex, $[(silox)_2TaH_2]_2$ (**11**). Exposure of **11** to ~1.0 equiv of carbon monoxide at –78 °C afforded the methylene dihydride complex, $[(silox)_2TaH]_2(\mu\text{-}CH_2)(\mu\text{-}O)$ (**19**), in 67% yield as an off-white powder. The purity of **19** was typically 95% (^1H NMR), and while it was thermally sensitive ($t_{1/2}$(decomposition) ≈ 3 h in benzene, $t_{1/2}$ ≈ 12 h in the solid state), it could be kept at –20 °C with minimal degradation. Quenching the methylene dihydride with an excess of HCl provided 2.2 equiv of H_2 and 0.75 equiv of CH_4, while hydrolysis with D_2O generated 1.8 equiv of dihydrogen (presumably HD). Mass spectral analysis of the 0.93 equiv of methane released indicated ≥80% CH_2D_2, ≤20% CH_3D, and a trace of CH_4. The hydrolysis data are consistent with electrophilic attack at the Ta–C bond by D^+ and a minor amount of D_2O-promoted reductive elimination. Addition of H_2O to $[(silox)_2TaD]_2(\mu\text{-}CD_2)(\mu\text{-}O)$ (**19**-d_4), prepared from **11**-d_4 and CO, generated similar ratios of CH_2D_2, CHD_3, and CD_4.

Methylene dihydride **19** exhibited two broad singlets at δ 15.99 and δ 7.08 in its ^1H NMR spectrum corresponding to the hydride and μ-CH_2 ligands, respectively. Infrared spectra revealed a terminal hydride stretch at 1792 cm^{-1} that shifted to 1285 cm^{-1} for **19**-d_4. Methylene dihydride prepared from ^{13}CO (**19**-^{13}C) manifested a resonance at δ 178.10 (J_{CH} = 135 Hz) in the ^{13}C NMR spectrum, comparable to the resonances of previously prepared μ-alkylidene species.[19] Assuming a relatively square $Ta_2(CH_2)O$ core, the structure of **19** probably consists of two trigonal bipyramids containing equatorial silox groups and axial hydrides adjoined by a diequatorial μ-oxo and diaxial μ-methylene. In one step, two of the crucial CO reduction steps have been effected. Since CO dissociation cannot occur across the Ta(IV) centers of **11**, it is clear that C–H bond formation must precede or accompany C–O bond scission.

Reformation of the C–O bond occurred when $[(silox)_2TaH]_2(\mu\text{-}CH_2)(\mu\text{-}O)$ (**19**) was subjected to a slight excess of CO at –78 °C. A formyl formaldehyde complex, $[(silox)_2TaH](\mu{:}\eta^2,\eta^2\text{-}CHO)(\mu{:}\eta^1,\eta^2\text{-}CH_2O)[Ta(silox)_2]$ (**20**), was isolated as a pale yellow powder in 55% yield and stored at –20 °C to prevent further reaction. A CO uptake from **19** of 1.0 equiv was measured, and **20** released 0.96 equiv of H_2 and 2.0 equiv of CH_3OH in separate quenching experiments using H_2O. The formyl formaldehyde was also prepared directly from $[(silox)_2TaH_2]_2$ (**11**) in greater isolated yield (79%) when a higher pressure of CO was used, and an uptake of 1.85 equiv of CO/mol of **11** was noted. Quenching with D_2O and subsequent methanol analysis by ^{13}C NMR indicated a rough 1:1 mixture of CHD_2OD and CH_2DOD, resulting from electrophilic cleavage of the μ-formyl and μ-formaldehyde, respectively. The labeled methanols appear as a rough 4:5:6:2:1 multiplet (J_{CD} ≈ 21 Hz) attributed to an overlapping 1:1:1 triplet and 1:2:3:2:1 pentet, the latter shifted by Δδ 0.42 because of an NMR isotope effect.[56]

The four inequivalent silox groups exhibited in the ^1H and ^{13}C NMR spectra testified to the asymmetry of $[(silox)_2TaH](\mu{:}\eta^2,\eta^2\text{-}CHO)(\mu{:}\eta^1,\eta^2\text{-}CH_2O)[Ta(silox)_2]$ (**20**), and previously identified μ-CHO (e.g., **18**) and η^2-CH_2O (e.g., **15**) ligands provided precedents for the remaining assignments. The inequivalent protons of μ-OCH_2 at δ 2.92 and δ 3.36 were coupled by 3.5 Hz, while the formyl singlet was found at δ 5.80. In the ^{13}C spectrum of **20**-$^{13}CHO/^{13}CH_2O$, the μ-formyl resonated as a doublet (J_{CH} = 166 Hz) at δ 134.94, and the μ-formaldehyde appeared as a triplet at δ 79.08 with J_{CH} = 159 Hz; no C–C coupling was observed. The ^1H NMR singlet at δ 14.99 was attributed to a terminal hydride, with its Ta–H stretch at 1774 cm^{-1} in the IR spectrum shifting to 1274 cm^{-1} upon deuteration. The structure of **20** shown in Scheme III is consistent with NOE experiments that suggest the TaH is proximate to the μ-OCH_2 and that one of the μ-formaldehyde protons is near the μ-CHO. Although the precise orientation of the ligands is unknown, the quenching and spectral data place the formulation of **20** on a firm basis. The molecule is portrayed such that each tantalum is six-coordinate, but the formaldehyde ligand may be a $\mu{:}\eta^1,\eta^1$-bridge, and the hydride may exist on the other tantalum with concurrent transposition of the formyl oxygen bonds. Similarly, the Ta–C and Ta–O formaldehyde bonds can be reversed, especially considering the propensity of related Zr–O–CHR–Zr (R = alkyl, H) bridges to undergo rapid 1,2-dyotropic shifts[76] that exchange bonds without reorienting the substituents.[75,77] Unfortunately, IR spectra of **20**, **20**-^{13}CHO, and **20**-$^{13}CHO/^{13}CH_2O$ failed to aid in the structure proof, presumably because critical CO bands were buried beneath intense silox absorptions (800–900 cm^{-1}).

Thermolysis of **20** for 1 h at 60 °C afforded light yellow $[(silox)_2Ta]_2(\mu\text{-}O)_2(\mu\text{-}CHMe)$ (**21**) in 61% isolated yield upon precipitation from hexanes. μ-Ethylidene **21** could be crystallized from hydrocarbons, but single crystals suitable for X-ray diffraction analysis were not obtained despite exhaustive efforts.

(75) Berno, P.; Floriani, C.; Chiesi-Villa, A.; Guastini, C. *J. Chem. Soc., Chem. Commun.* **1991**, 109–110. The structure of a $\mu{:}\eta^2,\eta^2$-CH_2O unit is included.

(76) Reetz, M. T. *Adv. Organomet. Chem.* **1977**, *16*, 33–65.

(77) (a) Gell, K. I.; Williams, G. M.; Schwartz, J. *J. Chem. Soc., Chem. Commun.* **1980**, 550–551. (b) Erker, G.; Kropp, K. *Chem. Ber.* **1982**, *115*, 2437–2446. (c) Erker, G.; Dorf, U.; Czisch, P.; Petersen, J. L. *Organometallics* **186**, *5*, 668–676.

It is reasonably stable, decomposing to undetermined products in solution at >90 °C; thus, satisfactory molecular weight and elemental analysis data were obtained. The μ-ethylidene ligand was characterized by a doublet and a quartet at δ 3.81 (3 H) and δ 5.51 (1 H) in the ^{1}H NMR spectrum, respectively, with ^3J = 7.4 Hz. The bridging carbon exhibited a ^{13}C resonance at δ 191.22 with coupling to the unique hydrogen (^1J = 109 Hz) and the methyl group (^2J = 7 Hz), which resonated at δ 25.67 (^1J = 128 Hz, ^2J = 4 Hz). Quenching **21** with excess H_2O provided 1.0 equiv of C_2H_6, which was identified by its infrared spectrum. Most importantly, material prepared from ^{13}CO (**21**-^{13}CH^{13}CH$_3$) exhibited a $^1J_{CC}$ of 36 Hz, characteristic of sp^3–sp^3 coupling.[70]

One curious feature of **21** concerns the equivalence of its silox ligands at 25 °C, which are diastereotopic in reference to the μ-ethylidene ligand. The silox resonance split at ca. –40 °C in the ^{1}H NMR spectrum, but at lower temperatures it became a broad singlet due to slow ^{t}Bu group rotation, a common occurrence in sterically encumbered systems.[44] The μ-ethylidene might rotate easily if an asymmetric [(silox)$_2$Ta=O](μ-O)[MeHC=Ta(silox)$_2$] (**21′**) structure were close in energy, providing a ready pathway for equilibration of the tantalum centers (cf. Figure 1). The observation of a normal ^3J of 7.4 Hz for the μ-CH(CH$_3$) fragment rules out rapid β-H elimination as the pathway for equilibration of the tantalum centers.

One final clean carbonylation product was obtained from extended exposure of either [(silox)$_2$TaH$_2$]$_2$ (**11**) or [(silox)$_2$TaH](μ:η^2,η^2-CHO)(μ:η^1,η^2-CH$_2$O)[Ta(silox)$_2$] (**20**) to 1 atm of CO. Thermally stable, colorless [(silox)$_2$Ta]$_2$(μ:η^1,η^1-CH=CHO)(μ:η^1,η^2-CH$_2$O)(μ-O) (**22**) was isolated in 50% yield upon precipitation from hexanes, and CO uptake experiments (2.60 equiv of CO per **11**) verified the composition. The ^{1}H NMR spectrum of **22** showed four different multiplets: two doublets at δ 3.79 and 3.97, exhibiting 2.9-Hz coupling, and another set of doublets at δ 7.04 and 8.43 with J = 7.5 Hz. The first set corresponds to the formaldehyde ligand that remained during the transformation from **20**, while the olefinic second group was assigned to a μ:η^1,η^1-CH=CHO bridge. Quenching studies again proved critical in identifying the molecule. Hydrolysis of **22** in THF provided a reproducible 1:1 ratio of methanol and acetaldehyde, consistent with the formulation, although the yields were only moderate (0.5–0.7 equiv per **22**).

Four inequivalent silox groups were observed by ^{13}C{^{1}H} NMR, and the ^{1}H-coupled spectrum of **22**-^{13}CH^{13}CHO/^{13}CH$_2$O helped to solidify the proposed structure. A triplet at δ 89.32 (J_{CH} = 158 Hz) was consistent with the μ-formaldehyde ligand, and olefinic multiplets at δ 162.40 ($^1J_{CH}$ = 181) and 167.18 (br, $^1J_{CH}$ = 141, $^2J_{CH}$ = 9 Hz) characterized the enolate fragment, which was further corroborated by a typical sp^2–sp^2 coupling of J_{CC} = 62 Hz.[70] A single-crystal X-ray structure determination of **22** was undertaken, but the disorder problems proved to be so severe that only the tantalum and silicon atoms and a three-atom bridge could be located. The IR spectra were informative, revealing an enolate ν(CC) band at 1509 cm^{-1} for **22** that shifted to 1458 cm^{-1} for **22**-^{13}CH^{13}CHO/^{13}CH$_2$O and a ν(CO/^{13}CO) absorption at 1218/1191 cm^{-1}.

Scheme III also provides mechanistic information concerning the course of CO reduction. When ^{13}CO was used to prepare [(silox)$_2$TaH]$_2$(μ-^{13}CH$_2$)(μ-O) (**19**-^{13}*C*) and the subsequent carbonylation was conducted with CO, the μ-formyl ligand of [(silox)$_2$TaH](μ:η^2,η^2-^{13}CHO)(μ:η^1,η^2-CH$_2$O)[Ta(silox)$_2$] (**20**-^{13}CHO) was consistently found to be >95% labeled. During the transformation, 20–70% of the label was also observed in the μ-CH$_2$O bridge. The labeled formaldehyde appears to depend on the amount of degradation taking place in the **19**-^{13}*C* to **20**-^{13}CHO conversion; the best yields of **20**-^{13}CHO corresponded to the lowest amount of μ-^{13}CH$_2$O present. Since no loss of label from the μ-^{13}CHO was found in any case, this label leakage into the formaldehyde position cannot result from decarbonylation of **19**-^{13}*C* to [(silox)$_2$TaH$_2$]$_2$ (**11**), because **11** would have reacted with CO to form some unlabeled **20**. The degradation product(s) of **19**-^{13}CO under CO must somehow serve as a spurious source of the μ-^{13}CH$_2$O. Likewise, when **19** was treated with ^{13}CO, the product **20**-^{13}CH$_2$O contained variable amounts of unlabeled μ-CH$_2$O.

The thermal conversion of **20**-^{13}CHO to [(silox)$_2$Ta]$_2$(μ-O)$_2$(μ-^{13}CHMe) (**21**-^{13}CHMe) occurred with no measurable label transfer into the Me group; hence, this process is clean. Reversal of the labeling scheme (**20**-^{13}CH$_2$O to **21**-CH^{13}CH$_3$) afforded consistent results. In summary, while minor scrambling of label occurs at the formyl formaldehyde (**20**) stage due to exchange with byproducts, the methylene of **19** becomes the formyl of **20**, which is ultimately transformed to the alkylidene carbon of **21**. Treatment of **20** with ^{13}CO afforded the formaldehyde enolate with label incorporation into the μ:η^1,η^1-OCH=CH bridge, but mechanistic assessment required the assignment of the enolate carbon resonances. Identification of the O-bound carbon via an NMR isotope shift was attempted by treating **11** with a 1:1 mixture of C^{18}O/CO for 10 min at 25 °C in benzene-d_6 to afford ^{18}O isotopomers of **22**. However, only the μ-CH$_2$O unit exhibited a measurable ^{13}C isotope shift ($\Delta\delta$ = 0.04).[10] Fortunately, hydrolysis of the product of **20** and ^{13}CO led to only H$_3$C^{13}CHO (>95%); hence, the final CO is incorporated into the oxygenated position of the TaO^{13}CH=CHTa bridge in [(silox)$_2$Ta]$_2$(μ:η^1,η^1-CH=^{13}CHO)(μ:η^1,η^2-CH$_2$O)(μ-O) (**22**-CH^{13}CHO).

Further mechanistic elucidation of the carbonylations of [(silox)$_2$TaH$_2$]$_2$ (**11**) proved to be elusive. Attempts to deuterate the hydride positions of methylene **19** or formyl formaldehyde **20** with D$_2$ or deuterated olefins led to degradation, and thermal probes of the molecules typically led to undesirable decomposition pathways. Although the primary focus of the carbonylation study concerned the transformations of **11** and subsequent products, the μ-oxo hydrides **12** and **14** were also briefly examined.

Treatment of [(silox)$_2$TaH]$_2$(μ-O)$_2$ (**12**) with a varied excess of carbon monoxide persistently yielded a mixture of products. The major product, formed in 70–95% yield by ^{1}H NMR, is formulated as [(silox)$_2$Ta]$_2$(μ-O)$_2$(μ-CH$_2$O) (**23**) on the basis of a CO uptake of ~1.1 equiv and spectral data indicative of inequivalent tantalum centers joined by a formaldehyde unit (eq 8). Its singlet at δ 4.33 in the ^{1}H NMR was corroborated by a

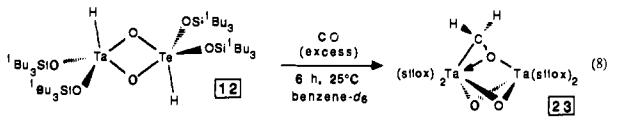

(8)

triplet in the ^{13}C NMR at δ 96.64 (J = 160 Hz) for **23**-^{13}*C*, prepared from **12** and ^{13}CO. Dioxo formaldehyde **23** could not be separated from the minor product, which was not identified. An aqueous quench of the mixture containing ~90% **23** yielded 0.67 equiv of MeOH, consistent with protolytic cleavage of the μ-CH$_2$O fragment. The observation of 2:1:1 silox resonances suggests that the tetrasiloxditantalum core remains static in relation to any movement of the formaldehyde bridge, depicted in a μ:η^1,η^2 binding mode.

Carbonylation (<1 atm of CO) of the isomer mixture of μ-oxo dihydrides [(silox)$_2$HTa]$_2$(μ-H)$_2$(μ-O) (**14**) provided off-white [(silox)$_2$HTa](μ-O)$_2$[TaMe(silox)$_2$] (**24**) in ~90% yield (eq 9).

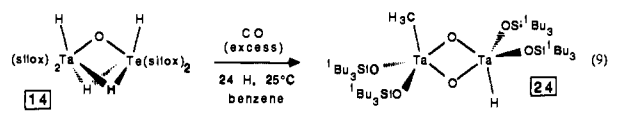

(9)

An uptake of 0.90 equiv of CO was measured, and TaCH$_3$ resonances were evident in ^{1}H (δ 1.52) and ^{13}C (δ 50.6, J_{CH} = 123 Hz) NMR spectra. An aqueous quench provided 1.0 equiv of CH$_4$ and 0.86 equiv of H$_2$. The observation of one sharp and one broad silox resonance in the ^{1}H NMR spectrum and at least three SiC signals in the ^{13}C{^{1}H} NMR spectrum suggests that

the molecule does not contain a mirror plane. Steric repulsions between the equatorial silox groups in the illustrated pseudo-C_{2h} core may desymmetrize **24**. Alternatively, methyl and/or hydride may occupy equatorial positions, leaving the less crowded axial sites for siloxes. Indications of similar structural anomalies are not observed in the related hydride dimer, $[(silox)_2TaH]_2(\mu\text{-}O)_2$ (**12**), which is presumably C_{2h}.

Three pieces of information led to the conclusion that $[(silox)_2HTa](\mu\text{-}O)_2[TaMe(silox)_2]$ (**24**) was a unique molecule and not a mixture of **12** and $[(silox)_2MeTa]_2(\mu\text{-}O)_2$. While the IR spectrum of **24** (ν(TaH) = 1804 cm^{-1}) could be virtually overlaid with that of **12**, mass spectral data were inconsistent with a mixture. A parent ion peak for the bis-μ-oxo hydrido methyl was observed at m/e 1270 (M^+), but the parent ion peak for **12**, centered at m/e 1255 ($(M-1)^+$), was absent. Secondly, a ^{13}C NMR sample of **24** was spiked with a small amount of **12**, and the critical SiC resonance of the latter was observed to be separate from the hydrido methyl. Finally, sealed NMR tube experiments showed that **24** was converted to ~90% $[(silox)_2Ta]_2(\mu\text{-}O)_2(\mu{:}\eta^1,\eta^2\text{-}MeCHO)$ (**25**) after about 6 days under excess CO at 25 °C (eq 10). In the ^1H NMR spectrum of **25**, four

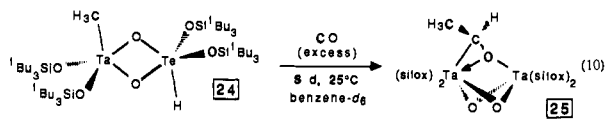

different silox resonances were accompanied by a doublet at δ 2.43 and a quartet at δ 5.04 (J = 6.3). Synthesis of **25**-$H_3{}^{13}C{}^{13}CHO$ permitted identification of the aldehyde carbon (δ 110.11, J_{CH} = 157 Hz) and its methyl substituent (δ 21.71, J_{CH} = 126 Hz) and revealed a 37.8-Hz carbon–carbon coupling consistent with an sp^3–sp^3 bond.[70] Hydrolysis of **26** in THF-d_8 yielded ethanol (^1H NMR), as expected for electrophilic attack at the aldehydic Ta–C bond. Carbonylation of a 1:1 mixture of $[(silox)_2TaH]_2(\mu\text{-}O)_2$ (**12**) and $[(silox)_2TaCH_2CH_3]_2(\mu\text{-}O)_2$ (**13**) afforded products derived only from **12**; the bis-μ-oxo diethyl complex was unreactive, consistent with the postulation that the bis-μ-oxo hydrido methyl (**24**) is a unique molecule that produces **25** upon carbonylation. The conversion of **24** to **25** is believed to result from insertion of CO into the TaH (or TaMe) unit, followed by methyl (or hydride) transfer to the intermediate formyl (or acyl).

Discussion

Consequences of Silox Ligation. The hard, electronegative character of the oxygen-donating silox ligand[35] helps to establish the metal-centered electrophilicity critical to carbonylation and dihydrogen exchange chemistry. The facile process that interchanges tantalum hydride bonds with those of dihydrogen is best viewed as a σ-bond metathesis mechanism,[63] commensurate with the electrophilicity of the 16e$^-$ (**2**) or 14e$^-$ (**11**) tantalum centers, assuming silox is best treated as a 3e$^-$ donor. While this can be shown directly in the case of $(silox)_3TaH_2$ (**2**), which initially generates HD upon treatment with D_2, it must be inferred from magnetization transfer experiments on $[(silox)_2TaH_2]_2$ (**11**), since the speed of the reaction prohibits a similar labeling experiment.

Steric influences of $^tBu_3SiO^-$ [44] also contribute to the observed chemistry by inhibiting the oligomerization of low-coordinate molecules. The tris-silox coordination sphere permits the preparation of monomeric hydrides, while tantalums ligated by two siloxes have all been incorporated into dimeric frameworks. Steric factors also dominate the structural and dynamic properties of the hydrides and carbonylation products, especially in the ditantalum systems. The D_{2d} symmetry and the unbridged Ta–Ta bond of $[(silox)_2TaH_2]_2$ (**11**) are direct ramifications of the packing of the silox ligands. The two isomers of $[(silox)_2TaH]_2(\mu\text{-}H)_2(\mu\text{-}O)$ (**14a,b**) interconvert, but the C_2 disposition of the silox ligands in each creates a substantial barrier to the symmetrization process. Moreover, the ability of a $(silox)_2Ta$ fragment to interlock with another $Ta(silox)_2$ unit spanned by two or three bridging groups often results in inequivalence of the silox resonances in ^1H and ^{13}C NMR spectra. As a consequence, although the composition and molecular connectivities of the carbonylation products are evident from spectral and quenching studies, the exact stereochemistry remains somewhat ambiguous. The problem is compounded by the penchant of the silox resonances in both ^1H and ^{13}C NMR spectra to overlap, as portions of Table IV reveal.

Carbonylation Reactions. The straightforward carbonylations of $(silox)_3TaHR$ (R = H, **2**; Et, **5**) to give the monomeric aldehyde complexes, $(silox)_3Ta(\eta^2\text{-}OCHR)$ (R = H, **15**; Et, **16**), are representative of all of the CO reductions. Carbon monoxide reacts rapidly with **2** and **5**, probably on the time scale of CO dissolution, according to sealed NMR tube experiments. Aldehyde formation can be construed as an insertion of CO into the Ta–H bond to generate a transient $RTa(\eta^2\text{-}CHO)$ species, followed by hydride/alkyl transfer,[23,68,69,71-73] or reductive elimination. In the dimeric cases, CO insertions were similarly fast, but precipitation of carbonylation products enabled their isolation and characterization.

It is noteworthy that no acyl products have been observed in the presence of a tantalum hydride. For example, $(silox)_3HTa(\eta^2\text{-}OCEt)$ is a plausible intermediate on the path to **16**, one that might have been stable. The insertion of CO into a metal–hydride bond is considered to be kinetically competitive with insertion into a corresponding metal–alkyl bond,[74,78] but thermodynamically disfavored.[74,79,80] Consider a generic comparison of the two insertion processes indicated in eq 11 and 12. Since the heats of

$$M\text{–}H + CO \rightarrow M\text{–}CHO + \Delta H_{fmyl} \quad (11)$$

$$M\text{–}Me + CO \rightarrow M\text{–}CMeO + \Delta H_{acyl} \quad (12)$$

formation of $^\bullet$CHO (ΔH_f° = 7.2 kcal/mol), $^\bullet$CMeO (ΔH_f° = –5.4 kcal/mol), $^\bullet CH_3$ (ΔH_f° = 34 kcal/mol), and $^\bullet$H (ΔH_f° = 52 kcal/mol) are known,[81] an expression for $\Delta H_{fmyl} - \Delta H_{acyl}$ (eq 13) may be derived and simplified as shown (eq 14). Furthermore,

$$\Delta H_{fmyl} - \Delta H_{acyl} = [\Delta H_f^\circ(^\bullet CHO) - \Delta H_f^\circ(^\bullet CMeO)] - [\Delta H_f^\circ(^\bullet H) - \Delta H_f^\circ(^\bullet CH_3)] + [D(M\text{–}H) - D(M\text{–}Me)] - [D(M\text{–}CHO) - D(M\text{–}CMeO)] \quad (13)$$

$$\Delta H_{fmyl} - \Delta H_{acyl} = -5.4 + [D(M\text{–}H) - D(M - Me)] - [D(M\text{–}CHO) - D(M\text{–}CMeO)] \quad (14)$$

$$\Delta H_{fmyl} - \Delta H_{acyl} \approx -5.4 + [D(M\text{–}H) - D(M\text{–}Me)] \quad (15)$$

if $[D(M\text{–}CHO) - D(M\text{–}CMeO)]$ can be approximated as 0 kcal/mol, as would be the case if M were an organic fragment, then $\Delta H_{fmyl} - \Delta H_{acyl}$ depends only on the bond strengths of the metal–hydride and metal–alkyl involved (eq 15). Note that there is an inherent enthalpic bias of 5.4 kcal/mol *toward formation of the formyl* (this number will vary slightly depending on the acyl) that results from the greater strength of the C–H bond in $^\bullet$CHO (18.4 kcal/mol) vs the C–Me bond in $^\bullet$CMeO (13 kcal/mol).

While this bias is opposed by the greater strength of metal–hydride bonds over metal–carbon bonds, the bond strength difference is minimized in early transition metal and actinide

(78) Berke, H.; Hoffmann, R. *J. Am. Chem. Soc.* **1978**, *100*, 7224–7236.
(79) Halpern, J. *Acc. Chem. Res.* **1982**, *15*, 238–244.
(80) Conner, J. A.; Zafarani-Moattar, M. T.; Bickerton, J.; El Saied, N. E.; Suradi, S.; Carson, R.; Takhin, G. A.; Skinner, H. A. *Organometallics* **1982**, *1*, 1166–1174.
(81) (a) Benson, S. W. *THermochemical Kinetics*; Wiley & Sons: New York, 1968. (b) Kerr, J. A. *Chem. Rev.* **1966**, *66*, 465–500.

Scheme IV

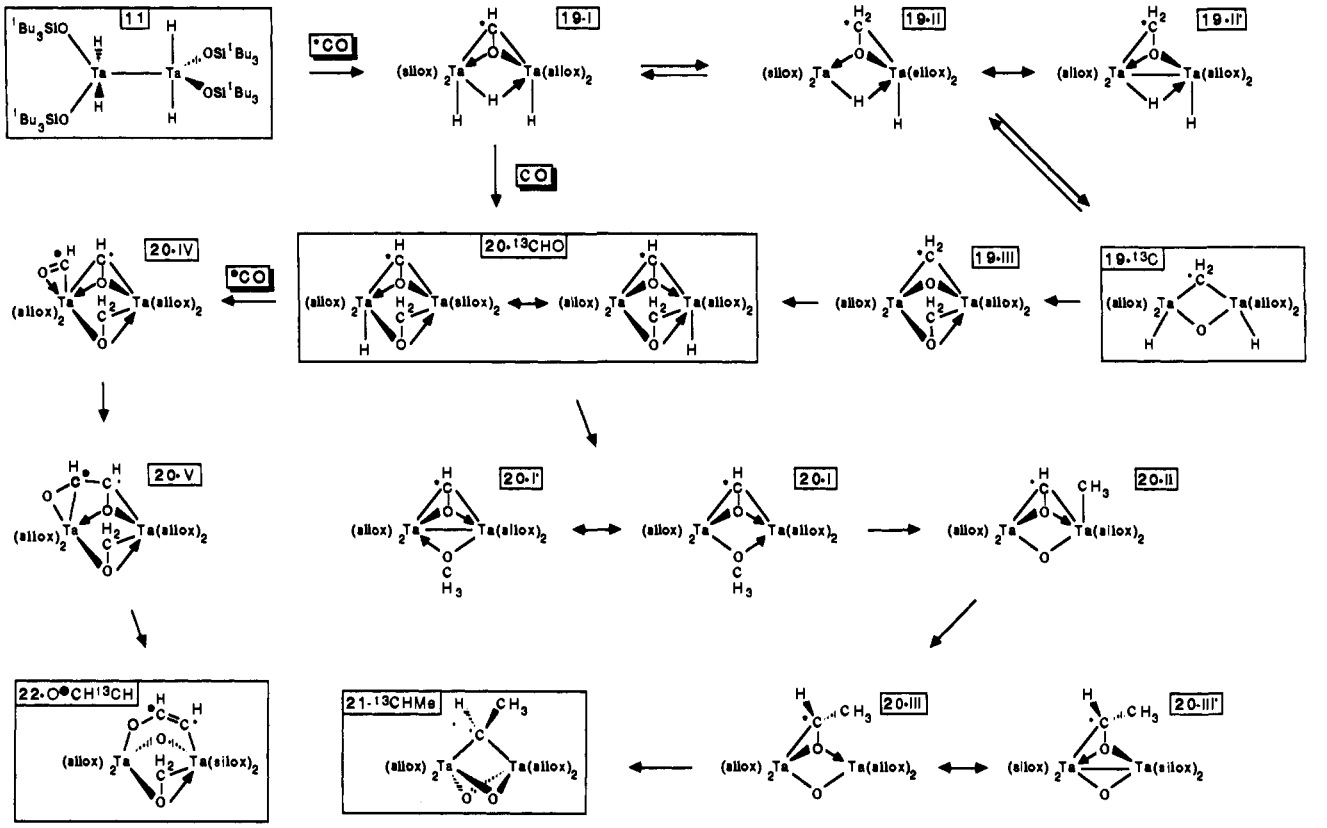

species;[40] thus, M–CHO formation in these systems becomes thermodynamically competitive with M–CRO production.[74] Additional thermodynamic factors become involved when early transition metal species form η^2-CHO and μ:η^2,η^2-CHO ligands;[23] these factors may favor bridging formyls over analogous acyls (i.e., the $[D(\text{M–CHO}) - D(\text{M–CMeO})] \approx 0$ approximation may be invalid). Coupled with lower kinetic barriers for hydride vs alkyl migration,[74,78] there are clear reasons to suspect that the carbonylation chemistry herein is dominated by chemistry derived from CO insertion into Ta–H bonds. Every carbonylation product observed in this study can be so rationalized.

The complicated transformations that occur upon carbonylation of $[(\text{silox})_2\text{TaH}_2]_2$ (**11**) bear further scrutiny, since the isolation of intermediates and the ^{13}CO-labeling studies permit some mechanistic evaluation. Scheme IV presents a proposed pathway for the breakdown of carbon monoxide by **11**, tracing the fate of the first *CO as determined from the labeling experiments. Consider first the generation of $[(\text{silox})_2\text{TaH}]_2(\mu\text{-H})(\mu{:}\eta^2,\eta^2\text{-CHO})$ (**19-I**), since this μ:η^2,η^2-formyl is structurally analogous to $[(\text{silox})_2\text{TaCl}]_2(\mu\text{-H})(\mu{:}\eta^2,\eta^2\text{-CHO})$ (**18**). At this point, the scheme partitions: with **11** plus 1 equiv of *CO, μ-methylene **19-**^{13}C is formed, indicating that **11** reacts with carbon monoxide faster than **19-I**. Reductive elimination of the μ:η^2,η^2-formyl and hydride ligands generates $[(\text{silox})_2\text{TaH}](\mu\text{-H})(\mu{:}\eta^2,\eta^1\text{-CH}_2\text{O})[\text{Ta(silox)}_2]$, a bridging formaldehyde species that can be described as a Ta(III)/Ta(V) complex (**19-II**) or one containing a Ta(IV)–Ta(IV) bond (**19-II'**). This recurring ambiguity regarding the presence of a Ta–Ta bond is due to the valence bond formalism that aids in visualization of the σ-bonds in the system. Oxidative addition of the μ-formaldehyde C–O bond across the Ta(III) center in **19-II** affords $[(\text{silox})_2\text{TaH}]_2(\mu\text{-}^{13}\text{CH}_2)(\mu\text{-O})$ (**19-**^{13}C).

The pathway linking **19-**^{13}C to $[(\text{silox})_2\text{TaH}](\mu{:}\eta^2,\eta^2\text{-}^{13}\text{CHO})(\mu{:}\eta^1,\eta^2\text{-CH}_2\text{O})[\text{Ta(silox)}_2]$ (**20-**^{13}CHO) requires some pause, because a C–O bond is reformed. It is reasonable to propose that the formation of **19-**^{13}C from **19-I** is reversible, because the bridging oxygen atom *retains two bonds to the tantalums* in forming the bridging formyl. However, since the label of **19-**^{13}C does not scramble into the formaldehyde position of **20-**^{13}CHO, carbonylation of **19-I** cannot lead to symmetric bis-μ-formyl or bis-formaldehyde intermediates. Alternatively, carbonylation of **19-**^{13}C may yield a bridging formaldehyde complex, $[(\text{silox})_2\text{Ta}]_2(\mu\text{-}^{13}\text{CH}_2)(\mu\text{-O})(\mu\text{-OCH}_2)$ (**19-III**), that precedes the reformation of the formyl C–O bond in **20-**^{13}CHO. Recall that carbonylation of $[(\text{silox})_2\text{TaH}]_2(\mu\text{-O})_2$ (**12**) proceeded in a similar manner to yield $[(\text{silox})_2\text{Ta}]_2(\mu\text{-O})_2(\mu\text{-CH}_2\text{O})$ (**23**).

The conversion of **20-**^{13}CHO to the μ-ethylidene **21-**^{13}CHMe is more complex. While **20-**^{13}CHO is drawn with both metal centers six-coordinate, hydride migration is feasible via the bond shifts shown. With the hydride on the tantalum containing both Ta–CHO and Ta–CH_2O bonds, only a reductive elimination with the methylene is productive. Elimination with the TaCHO unit would lead to a symmetric bis-formaldehyde intermediate and ruin the integrity of the label transfer to **21-**^{13}CHMe. There is some rationale for this discrimination: NOE experiments on **20** suggested that the hydride is proximate to one of the formaldehyde hydrogens, while the formyl is near the other. In addition, the bridging configuration of the μ:η^2,η^2-CHO group may render it less reactive than the μ-formaldehyde. Formaldehyde hydride reductive elimination leads to Ta(III)/Ta(V) **20-I** (alternatively, Ta(IV)/Ta(IV) **20-I'**).[67] Oxidative addition of the O–CH_3 bond to the Ta(III) center produces μ-formyl methyl **20-II**, which subsequently undergoes reductive elimination to Ta(III)/Ta(V) μ-aldehyde **20-III** (or Ta(IV)/Ta(IV), **20-III'**). Finally, reductive deoxygenation of **20-III** yields the μ-ethylidene **21-**^{13}CHMe. Instead of **20-I** → **20-II**, oxidative addition of the formyl C–O bond could occur, but that would require addition of the OCH_3 unit across a Ta—C(H)=Ta bridge, a reaction without substantial precedent.

The thermal conversion of **20-**^{13}CHO to **21-**^{13}CHMe requires a significant amount of time, ~36 h at 25 °C, yet no intermediate was detected by NMR spectroscopy, suggesting that the initial elimination step is slow relative to subsequent CO addition[67] and CC elimination events. This seems strange, given the notable

Scheme V. Fischer–Tropsch Mechanism Depicting $(CH_3O)_s$, $(CH_2O)_s$, $(CHO)_s$, and Other Adsorbed Oxygenates in Equilibrium with Related Hydrocarbyl Fragments

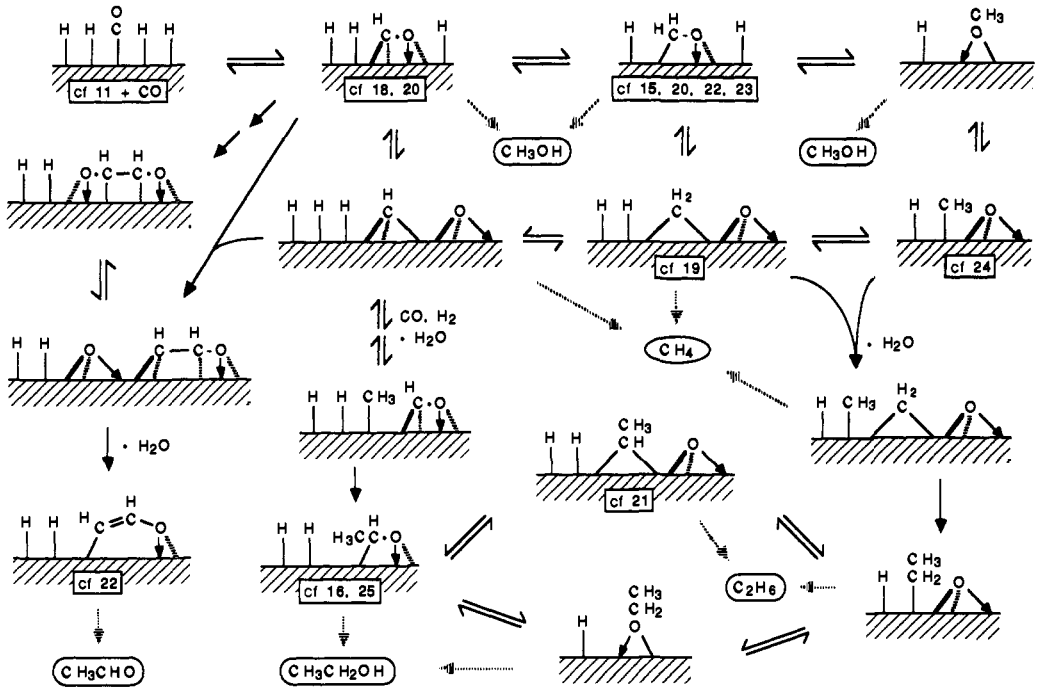

lack of systems that display either process cleanly. It may be more appropriate to view the oxidative addition as a nucleophilic attack by the tantalum on the C–O bond,[37] since O(pπ) → Ta(dπ) bonding should make the oxygen a good leaving group. The C–C coupling can be alternately envisaged as a migration of the methyl to a receptor p-orbital on the formyl,[68,69] and the possibility that the **20**-^{13}CHO to **20**-II conversion is reversible cannot be discounted. The carbonylation of $[(silox)_2HTa]_2(\mu\text{-}H)_2(\mu\text{-}O)$ (**14**) to give $[(silox)_2HTa](\mu\text{-}O)_2[TaMe(silox)_2]$ (**24**) is probably analogous to the **19**-I to **20**-II conversion, since carbonylation of a Ta_2H_3 fragment leads to a $Ta_2(\mu\text{-}O)Me$ moiety in both instances.

One further comment about the overall scheme should be emphasized. During the course of conversion of $[(silox)_2TaH_2]_2$ (**11**) to $[(silox)_2Ta]_2(\mu\text{-}O)_2(\mu\text{-}^{13}CHMe)$ (**21**-^{13}CHMe), the proposed mechanism permits each oxygen to be bound to two tantalums *throughout the entire scheme*. Since early transition metal–oxygen bonds are known to be extremely strong,[9,40] the energy requirements for breaking such interactions during the course of CO reduction would be incommensurate with the ease of CO insertion and deoxygenation.

Minimal information is available about the carbonylation (•CO = CO or ^{13}CO) of $[(silox)_2TaH](\mu\text{:}\eta^2,\eta^2\text{-}^{13}CHO)(\mu\text{:}\eta^1,\eta^2\text{-}CH_2O)[Ta(silox)_2]$ (**20**-^{13}CHO) to tantallaenolate $[(silox)_2Ta]_2(\mu\text{:}\eta^1,\eta^1\text{-}^{13}CH{=}{\bullet}CHO)(\mu\text{:}\eta^1,\eta^2\text{-}CH_2O)(\mu\text{-}O)$ (**22**-^{13}CH•CHO). In accord with the above arguments, Scheme IV portrays the conversion via initial CO insertion into the Ta–*H* bond to give **20**-IV, although CO insertion into the $\mu\text{:}\eta^2,\eta^2$-formyl Ta–C bond is a viable alternative. Subsequent C–C bond formation (**20**-V) and deoxygenation steps provide **22**-^{13}CH•CHO in a straightforward manner. In any mechanism invoking **20**-V or related bis-formyl, dynamic processes involving its CHO fragments cannot symmetrize the tantalum centers, because such an event would lead to scrambling of the label in the enolate bridge.

Conclusions

In viewing the relationship of these carbonylations to reactions occurring during Fischer–Tropsch (F-T) synthesis, it is important to recognize that the electropositive character of tantalum leads to the formation of strong Ta–O bonds,[9] providing much of the thermodynamic impetus for these transformations. The robust nature of these bonds also hampers catalysis, since hydrogenation of Ta–O bonds is expected to be difficult. Coupled with the noted stability of tantalum carbides,[82] the likelihood of the development of heterogeneous or homogeneous F-T catalysts based solely on tantalum and its oxides or carbides must be considered remote. For the tantalum work to be relevant, an important assumption must be stated: the CO reduction chemistry herein can be considered to model high-temperature (200–300 °C) and high-pressure (>100 atm) F-T processes,[1-7] provided the exothermic bias of creating Ta–O bonds translates into lower kinetic barriers for transformations common to those occurring on heterogeneous surfaces of true catalysts.

Given that assumption, the critical bond-breaking (C–O) and bond-making (C–H, C–C) events in the F-T sequence are illustrated in the carbonylation chemistry of $[(silox)_2TaH_2]_2$ (**11**). What distinguishes **11** from the majority of early transition metal and actinide hydrides that reduce CO without C–O bond scission[23-25] is its capability of serving as a 2e$^-$ reductant.[9-11] The electrons included in the Ta–Ta bond enable the molecule to react as a reducing agent, yet the tantalums are still very electrophilic because the metal–metal bond is not diffuse. In a sense, tetrahydride **11** serves as a more effective model for heterogeneous F-T catalysts, which typically comprise a group 8 or 9 metal or metal oxide in combination with a Lewis acidic support.

Scheme V illustrates a scenario for the F-T process that incorporates the mechanistic and structural information gained from the carbonylations of all of the hydride complexes. Beneath certain depictions are references to the tantalum compounds containing similar fragments. All C–C-bond-forming events are shown as irreversible because C–C-bond-breaking reactions have not been observed in the models. In addition, the transformations are treated as 2e$^-$ changes akin to oxidative addition/reductive elimination reactions and insertions.

Three main points can be drawn from the modeling studies. First, hydride transfer to CO concomitant with or prior to C–O bond scission[22] remains a reasonable alternative to CO dissociation[9-15] on surfaces containing adsorbed hydrogen. The ready carbonylation of $[(silox)_2TaH_2]_2$ (**11**) to $[(silox)_2TaH]_2(\mu\text{-}$

(82) Benziger, J. B. *Appl. Surf. Sci.* **1980**, *6*, 105–121.

CH_2)(μ-O) (**19**) serves as a primary example. The generation of formaldehyde complexes (silox)$_3$Ta(η^2-OCH$_2$) (**15**) and [(silox)$_2$Ta]$_2$(μ-O)$_2$(μ-CH$_2$O) (**23**) from (silox)$_3$TaH$_2$ (**2**) and [(silox)$_2$TaH]$_2$(μ-O)$_2$ (**12**) also emphasizes this proposition, as does the formation of hydrido methyl [(silox)$_2$HTa](μ-O)$_2$-[TaMe(silox)$_2$] (**24**) from treatment of [(silox)$_2$HTa]$_2$(μ-H)$_2$(μ-O) (**14**) with CO. Formyls [(silox)$_2$TaCl]$_2$(μ-H)(μ:η^2,η^2-CHO) (**18**) and [(silox)$_2$TaH](μ:η^2,η^2-CHO)(μ:η^1,η^2-CH$_2$O)[Ta(silox)$_2$] (**20**) also result from initial hydride transfer to CO.

Second, recall that the conversion of **19** to **20** required the reformation of the carbon–oxygen bond previously severed during the initial carbonylation of **11**. This surprising reversibility has important implications concerning the relationship between hydrocarbons and oxygenates in the F-T process. Oxygenated catalyst surfaces may serve as reservoirs for CH_{ads}, CR_{ads}, $(CH_2)_{ads}$, $(CHR)_{ads}$, $(CH_3)_{ads}$, and R_{ads} functionalities via OCH_{ads}, OCR_{ads}, $(OCH_2)_{ads}$, $(OCHR)_{ads}$, $(OCH_3)_{ads}$, and OR_{ads} adsorbates. This relationship between hydrocarbyl and oxygenate fragments is indicated via the equilibria in Scheme V, where single C–O-bond-breaking and -bond-making steps serve to separate the various functionalities. Methylene units that ultimately yield hydrocarbons are not constrained to be solely metal-bound on the catalyst surface. Typical F-T catalysts are empirically determined mixtures of metal oxides and support materials; thus, it is not a revelation to propose that surface oxides may play a major role in product formation, particularly in the generation of oxygenates. It is conceivable that oxygen coverages could be tuned for a particular distribution of products.[83]

Finally, removal of the oxygenate and hydrocarbyl adsorbates in the presence of hydrogen can be accomplished via reductive elimination reactions, illustrated by the dashed arrows in Scheme V. The surface-bound functionalities depicted have been constrained to include only C_1 and C_2 precursors, due to their proposed relationship with **11-25**. All of the products indicated have also been obtained from protolytic quenching of appropriate model complexes, showing the relationship of proton transfer to hydrogenation.

Experimental Section

General Considerations. All manipulations were performed using either glovebox or high vacuum line techniques. Hydrocarbon solvents containing 1–2 mL of added tetraglyme and ethereal solvents were distilled under nitrogen from purple benzophenone ketyl and vacuum-transferred from the same prior to use. CCl_4 was dried over P_2O_5 and vacuum-transferred from activated 4-Å molecular sieves. Benzene-d_6 and methylcyclohexane-d_{14} were dried over activated 4-Å molecular sieves, vacuum-transferred, and stored under N_2; toluene-d_8 and THF-d_8 were dried over sodium benzophenone ketyl. All glassware was oven-dried, and NMR tubes were additionally flamed under dynamic vacuum. Carbon monoxide (Matheson) and ^{13}CO (Cambridge) were used as received. Purification of $TaCl_5$ (Alfa) was accomplished via sublimation (10^{-4} Torr, 120 °C) and Na(silox),[35] (silox)$_3$TaCl$_2$ (**1**), (silox)$_3$Ta (**3**),[9] and (silox)$_2$TaCl$_3$ (**9**)[44] were prepared according to published procedures.

NMR spectra were obtained using Varian XL-200, XL-400, VXR-400S and Bruker AF-300 spectrometers. Variable-temperature ^{29}Si{^{1}H} and ^{1}H NMR spectra (supplementary material) were conducted on the XL-400 instrument. Line-shape analyses were performed using a modified version of DNMR3H.[84] Magnetization transfer NMR experiments were carried out on a Nicolet NT-360 instrument. Chemical shifts are reported relative to TMS and all couplings are in hertz. Infrared spectra were recorded on a Mattson FT-IR interfaced to an AT&T PC7300 computer or on a Perkin-Elmer 299B spectrophotometer. Gas chromatographic analyses were conducted on a Hewlett-Packard 5890 machine equipped with a 3392A integrator. For all runs, response factors were calibrated vs a standard reference, typically acetone. Elemental analyses were performed by Analytische Laboratorien, Elbach, West Germany, or Oneida Research Services, Whitesboro, NY. Mass spectrometry was performed at the Cornell University or University of Illinois facilities; Nujol (FAB-MS matrix) was dried over sodium and stored under N_2. Molecular weights were determined by benzene cryoscopy on a home-built device.

Procedures. 1. (silox)$_3$TaH$_2$ (2). To a flask containing (silox)$_3$TaCl$_2$ (**1**) (1.500 g, 1.672 mmol) and Na/Hg (0.9%, 17 g, 6.7 mmol) was added 30 mL of THF at –78 °C. The solution was placed under 1 atm of H_2 and warmed to 25 °C with stirring. After 24 h, the THF was removed to leave a gummy yellow-brown solid and Na/Hg, which was poured off. The residue was taken up in 8 mL of hexanes, and the resulting slurry was filtered. The collected solid was washed with 2 × 4 mL portions of hexanes, and the solution was cooled to –78 °C, yielding 590 mg of colorless, microcrystalline **2** (43%). When synthesized directly from (silox)$_3$Ta (**3**), dihydride **2** was prepared in ~80% yield.[9] UV–vis: 218 nm ($\epsilon \approx 5100$ M^{-1} cm^{-1}), 278 (4400). Anal. Calcd for $C_{36}H_{83}O_3Si_3Ta$: C, 52.14; H, 10.09. Found: C, 51.90; H, 10.05.

2. (silox)$_3$TaH$_2$ (2) + 2HCl. Into a flask containing 100 mg of **2** (0.121 mmol) was distilled 15 mL of Et$_2$O at –78 °C. HCl gas (0.24 mmol) was admitted to the flask via a gas bulb, and the reaction was allowed to stir for 1 h at –78 °C and 1 h at 25 °C. The volatiles were removed and passed through three 77 K traps prior to collection of 0.22 mmol of H_2 (1.8 equiv) via a Toepler pump. ^{1}H NMR analysis of the solid residue revealed 95% **1**, 5% **6**-Cl, and 5% (silox)H.

3. (silox)$_3$HTaEt (5). A flask containing **2** (800 mg, 0.965 mmol) and 20 mL of hexanes was exposed to ethylene (390 Torr, 1.93 mmol) from a calibrated gas bulb (91.0 mL). The solution was stirred for 5 h at 25 °C, filtered, and concentrated to 2 mL. Cooling the solution to –78 °C afforded colorless crystals (520 mg, 63%) that were collected by filtration and dried *in vacuo*. IR (Nujol): ν(TaH) 1794 cm^{-1}. Anal. Calcd for $TaSi_3O_3C_{38}H_{88}$: C, 53.24; H, 10.23. Found: C, 53.15; H, 10.15.

4. (silox)$_3$TaHCl (6-Cl). Into a flask containing **2** (500 mg, 0.605 mmol) was distilled 30 mL of CCl_4 at –78 °C. The solution was warmed to 25 °C and stirred for 1.5 h. After the solution was concentrated to dryness, the residue was dissolved in 4 mL of hexanes, filtered, and cooled to –78 °C to give 340 mg (63%) of colorless microcrystals that were collected by filtration. Anal. Calcd for $TaSi_3O_3ClC_{36}H_{82}$: C, 50.06; H, 9.57. Found: C, 50.04; H, 9.40.

5. (silox)$_3$TaHI (6-I). A flask containing **2** (700 mg, 0.844 mmol) and 25 mL of Et$_2$O at –78 °C was exposed to CH_3I (311 Torr, 0.851 mmol) from a calibrated gas bulb (50.4 mL). Gas, presumably CH_4, evolved as the solution was stirred and warmed to 25 °C. After stirring for 1.5 h, the solution was evaporated to dryness. The residue was dissolved in ~10 mL of hexanes, filtered, reduced in volume to ~5 mL, and cooled to –78 °C to provide 495 mg (62%) of colorless microcrystals that were collected by filtration. Anal. Calcd for $TaSi_3O_3IC_{36}H_{82}$: C, 45.27; H, 8.65. Found: C, 45.09; H, 8.55.

6. [(silox)$_3$TaH]$_2$(μ:η^1,η^1-CH$_2$(CH$_2$)$_3$O) (7). To a flask containing **6**-I (270 mg, 0.283 mmol) and 0.9% Na/Hg (1.110 g, 0.435 mmol of Na) was added 8 mL of THF at –78 °C. Warming the solution to 25 °C and stirring for 30 min produced a dark green color, which then faded to yellow while stirring for 4 h. The solution was concentrated to dryness and residual THF was removed by codistillation with pentane. The residue was dissolved in pentane and filtered, giving a pale yellow solution and a gray solid. Concentration of the solution to 1 mL, cooling to –78 °C, and filtration yielded an off-white powder (143 mg, 58% yield). Anal. Calcd for $Ta_2Si_6O_7C_{76}H_{172}$: C, 52.80; H, 10.03. Found: C, 52.78; H, 9.77.

7. [(silox)$_2$TaCl]$_2$(μ-H)$_2$ (10). a. To a 100-mL flask containing **11** (1.190 g, 0.969 mmol) was added 50 mL of Et$_2$O at –78 °C. The mixture was warmed to dissolve all of the solid, recooled to –78 °C, and exposed to 2 equiv of HCl (1.93 mmol) admitted via a gas bulb. Upon addition of HCl, the orange solution became a deep violet and effervesced vigorously. The solution was stirred for 1 h at –78 °C and 1 h at 25 °C, and then the solvent was removed. The dark violet residue was filtered in 5 mL of hexanes, which was then removed. The addition of 5 mL of THF and cooling to –78 °C resulted in violet crystals, which were isolated via filtration and washed with 2 mL of cold THF (980 mg, 78%).

b. A similar procedure on 200-mg scale (**10**) was analyzed via a Toepler pump, and 2.0 equiv of H_2 was released. Anal. Calcd for $Ta_2Cl_2Si_4O_4C_{48}H_{110}$: C, 44.47; H, 8.55; Cl, 5.47. Found: C, 44.63; H, 8.41; Cl, 5.49.

8. [(silox)$_2$TaH$_2$]$_2$ (11). To a 600-mL glass bomb reactor containing (silox)$_2$TaCl$_3$ (**9**) (12.55 g, 17.5 mmol) and 0.9% Na/Hg (270.5 g, 105

(83) For a view featuring differentiation of oxygenate and hydrocarbon pathways, see: (a) Miller, D.; Moskovits, M. *J. Am. Chem. Soc.* **1989**, *111*, 9250–9252. (b) Robbins, J. L.; Marucchi-Soos, E. *J. Phys. Chem.* **1989**, *93*, 2885–2888.

(84) Stempfle, W.; Klein, J.; Hoffmann, E. G. QCPE Program No. 450.

mmol (Na)) was distilled 75 mL of toluene at −78 °C. The bomb was cooled to 77 K and 1 atm of H_2 was admitted. After the bomb was sealed and warmed to 25 °C, the solution was stirred for 5 days, during which time a dark purple and then dark orange color developed. The solution was degassed, H_2 was readmitted (1 atm at 77 K), and stirring was resumed. After an additional 10 days, the toluene was removed under vacuum and as much Hg was decanted as possible. The residue was repeatedly extracted with 20-mL portions of hexanes, which were centrifuged under an N_2 atmosphere and decanted to give a deep orange solution. After filtration of the solution, the hexanes were removed in vacuo and replaced by 35 mL of Et_2O. Cooling the solution to −78 °C and filtration yielded orange crystals, which were dried *in vacuo* (8.92 g, 83% yield). ^1H NMR (C_7D_8, 25 to −80 °C): δ 12.06 (s, TaH), silox protons broadened due to slow rotation at low temperatures. ^{29}Si NMR: δ 14.14 (selective decoupling experiments indicated $J_{SiH(Ta)} \approx 0$) (C_7D_8, −70 °C) δ 12.11. M_r calcd 1228, found 1240. Anal. Calcd for $Ta_2Si_4O_4C_{48}H_{112}$: C, 46.96; H, 9.20. Found: C, 46.72; H, 9.03.

9. [(silox)$_2$TaH$_2$]$_2$ (11) + 6 HCl. Into a flask containing 200 mg of **11** (0.163 mmol) was distilled 10 mL of Et_2O at −78 °C, followed by 6 equiv of HCl (0.972 mmol) which was admitted via a gas bulb. The reaction was allowed to warm to 25 °C and stir for 2 h. The volatiles were removed and passed through three 77 K traps prior to collection of 0.783 mmol of H_2 (4.8 equiv) via a Toepler pump. The colorless crystalline residue was identified as (silox)$_2$TaCl$_3$ by ^1H NMR (>95%).

10. [(silox)$_2$TaD$_2$]$_2$ (11-*d*$_4$). All glassware was rinsed with D_2O prior to use. A glass bomb reactor containing [(silox)$_2$TaH$_2$]$_2$ (**11**) (2.00 g, 1.63 mmol) and 30 mL of toluene at 25 °C was exposed to 1 atm of D_2. At 1-h intervals, the solution was degassed and fresh D_2 was placed over the solution. After stirring for a total of 8 h, the solution was filtered and the toluene was removed *in vacuo*. Crystallization from 8 mL of Et_2O at −78 °C afforded 1.63 g of orange crystals of **10-*d*$_4$** (82% yield) with ~1–5% residual H, depending on the preparation.

11. [(silox)$_2$TaH]$_2$(μ-O)$_2$ (12). A flask containing **11** (405 mg, 0.330 mmol) and 15 mL of hexanes at −78 °C was opened to a calibrated gas bulb (50.1 mL) containing O_2 (120 Torr, 0.33 mmol). Upon warming to 25 °C, discharge of the orange color occurred with concomitant gas evolution. Stirring at 25 °C for 40 min afforded a colorless solution that was degassed with the Toepler pump, yielding 71 Torr of gas collected in a 78-mL volume (0.301 mmol). The gas was converted to H_2O upon circulation over CuO (300 °C), indicating an uptake of 1.0 equiv of O_2 and release of 0.91 equiv of H_2. An NMR spectrum of the residue indicated quantitative conversion. IR (hexanes): ν(TaH/D) 1808/1297, ν(Ta^{16}O/Ta^{18}O) 921/883, 803/766, 704/674 cm^{-1}. M_r found 1290, calcd 1258. FAB-MS (Nujol): *m/e* 1255 (53.3), 1256 (38.0), 1257 (23.0), 1258 (14.5). Anal. Calcd for $Ta_2Si_4O_6C_{48}H_{110}$: C, 45.84; H, 8.82. Found: C, 45.67; H, 8.40.

12. [(silox)$_2$TaCH$_2$CH$_3$]$_2$(μ-O)$_2$ (13). A flask containing **12** (300 mg, 0.238 mmol) and 10 mL of hexanes was exposed to excess ethylene (300 Torr) from a vacuum manifold. After stirring for 8 h at 25 °C, the solution was degassed and filtered. Crystallization from Et_2O at −78 °C afforded 120 mg of white crystals (39% yield). M_r found 1298, calcd 1313.

13. [(silox)$_2$TaH]$_2$(μ-H)$_2$(μ-O) (14). Into a flask containing 1.50 g of **11** (1.22 mmol) and $(CH_3)_3NO$ (92 mg, 1.23 mmol) was distilled 30 mL of Et_2O at −78 °C. As the deep orange suspension was stirred at 25 °C for 4 h, the color slowly discharged to give a pale brown solution. After filtration, concentration of the solution and cooling to −78 °C yielded white crystals that were collected by filtration and dried *in vacuo* (1.20 g, 67% yield). IR (Nujol): ν(TaH/D) 1834/1313, 1779/1275, 1345($\nu_{1/2}$ = 98 cm^{-1})/985. Anal. Calcd for $Ta_2Si_4O_5C_{48}H_{112}$: C, 46.36; H, 9.08. Found: C, 46.94; H, 8.99.

14. (silox)$_3$Ta(η^2-OCH$_2$) (15). To a flask containing **2** (400 mg, 0.483 mmol) and 15 mL of toluene at 25 °C was admitted CO (0.503 mmol) via a calibrated gas bulb. After the mixture was stirred for 1 h, the toluene was removed, and the product was crystallized from 5 mL of Et_2O at −78 °C to give 320 mg of colorless crystals (77% yield). IR (**15**/**15-*d*$_2$**/**15-^{13}*C*$_1$**, cyclohexane) ν(H_2CO/D_2CO/$H_2{}^{13}CO$) 932/932/914, (CH_2/CD_2/$^{13}CH_2$ wag) 552, 502, 543, (H_2CO/D_2CO/$H_2{}^{13}CO$ rock (tentative)) 600, 588, 600 cm^{-1}. Anal. Calcd for $TaSi_3O_4C_{37}H_{83}$: C, 51.84; H, 9.76. Found: C, 51.92; H, 9.66. M_r found 830, calcd 856.

15. (silox)$_3$Ta(η^2-OCHC$_2$H$_5$) (16). a. A flask containing (silox)$_3$TaHEt (210 mg, 0.245 mmol) and 5 mL of toluene at 25 °C was exposed to an excess of CO (320 Torr) from a vacuum manifold. The solution was stirred for 2.5 h and concentrated to dryness. The residue was filtered in Et_2O, and 88 mg yellow powder was isolated by crystallization from 1 mL of Et_2O at −78 °C (41% yield).

b. To a flask containing (silox)$_3$Ta (489 mg, 0.581 mmol) was added 18 mL of hexanes at −78 °C. The solution was exposed to propanal (120 Torr, 0.593 mmol) from a calibrated gas bulb (91.0 mL), causing immediate discharge of the blue-green color. After stirring for 30 min at 25 °C, the solution was filtered and concentrated to dryness. Crystallization from 3 mL of Et_2O at −78 °C afforded 325 mg of white crystals (62% yield). Anal. Calcd for $TaSi_3O_4C_{39}H_{87}$: C, 52.91; H, 9.91. Found: C, 52.93; H, 9.73.

16. [(silox)$_2$TaCl]$_2$(μ-H)(μ:η^2,η^2-CHO) (18). a. Synthesis. To a 25-mL flask containing **10** (440 mg, 0.339 mmol) was added ~5 mL of Et_2O at −78 °C. The flask was opened to a manifold containing CO (215 Torr, ~8 equiv). After the mixture was stirred at −78 °C for 2 h, the resulting yellow slurry was filtered and dried briefly *in vacuo*, affording 250 mg (56% yield) of light yellow, thermally sensitive **18** (typically 90–95% pure) as a powder that was stored at −20 °C.

b. HCl quench. Into a flask containing 78 mg (0.060 mmol) of **18** was distilled ~8 mL of Et_2O at −78 °C. HCl (162 Torr, 0.180 mmol) was admitted via a gas bulb. Gas evolved while the solution was allowed to warm to 25 °C (0.5 h) and then stirred for 1.5 h. The gases were passed through three liquid nitrogen traps and collected via a Toepler pump (0.058 mmol, 0.97 equiv/**18**). The collected hydrogen was converted to water by cycling over CuO (300 °C), and the remaining volatiles were recollected (0.007 mmol; 0.051 mmol, 0.85 equiv of H_2 by difference).

c. Hydrolysis. Into a flask containing 117 mg of **18** (0.0883 mmol) was distilled ~3 mL of THF at −78 °C. The slurry was frozen at 77 K, and an excess of H_2O(g) was admitted via the vacuum manifold. Upon thawing, the pale yellow solution became colorless within 10 min. Acetone standard (65 Torr, 0.177 mmol) was admitted via a gas bulb. The flask was frozen at 77 K and then removed from vacuum. About 0.1 mL of H_2O was added with a small amount of NaCl, and the solution flask was stoppered with a septum cap and maintained at 0 °C during GC analysis. Compounds found: 0.85 equiv (0.075 mmol) of MeOH per **18** (acetone reference); 0.87 equiv (0.077 mmol) of MeOH found in another run using 123 mg of **18**.

17. [(silox)$_2$TaH]$_2$(μ-CH$_2$)(μ-O) (19). a. Synthesis. To a flask containing **11** (1.00 g, 0.815 mmol) was added ~7 mL of Et_2O at −78 °C. The flask was opened to a calibrated gas bulb containing CO (0.805 mmol). After the mixture was stirred at −78 °C for 6 h, the resulting pale yellow slurry was filtered and dried briefly *in vacuo*, affording 682 mg (67% yield) of off-white, thermally sensitive **19** (typically 90–95% pure, with **11** and **20** as common contaminants) as a powder that was stored at −20 °C. IR (Nujol): ν(TaH/D) 1792/1285 cm^{-1}.

b. HCl quench. Into a flask containing 128 mg (0.102 mmol) of **19** was distilled ~5 mL of hexane at −78 °C. Excess HCl (206 Torr, 1.02 mmol) was admitted via a gas bulb. Gas evolved while the solution was allowed to warm to 25 °C (0.5 h) and stirred for 0.5 h. The gases were passed through three liquid nitrogen traps and collected via a Toepler pump (0.302 mmol, 2.96 equiv/**18**). The collected hydrogen was converted to water by cycling over CuO (300 °C), and the remaining volatiles were recollected (0.75 equiv, 0.077 mmol of CH_4; 0.225 mmol, 2.2 equiv of H_2 by difference).

c. Hydrolysis. To a frozen pentane solution of **19** (175 mg, 0.139 mmol) was admitted excess D_2O (0.94 mmol) from a calibrated gas bulb. Gas was evolved as the solution was stirred for 1 h at 25 °C. The gases were passed through three liquid nitrogen traps and collected via a Toepler pump (0.38 mmol, 2.7 equiv/**19**). The collected hydrogen was converted to water by cycling over CuO (300 °C), and the remaining volatiles were recollected (0.93 equiv of MeH; 1.8 equiv of H_2 by difference). Mass spectral analysis of the residual gas indicated ≥80% CH_2D_2, ≤20% CH_3D, and a trace of CH_4.

18. [(silox)$_2$TaH](μ:η^2,η^2-CHO)(μ:η^1,η^2-CH$_2$O)[Ta(silox)$_2$] (20). a. Synthesis from 11. A flask containing **11** (609 mg, 0.496 mmol) in 4 mL of Et_2O was cooled to −78 °C and exposed to 1 atm of CO. While stirring at −78 °C for 8 h, the orange solution slowly bleached to give an off-white slurry. Filtration and brief drying *in vacuo* gave 500 mg of white powder (79% yield) that was stored at −20 °C. IR (Nujol): ν(TaH/D) 1774/1274 cm^{-1}.

b. Synthesis from 19. To a flask containing **19** (250 mg, 0.199 mmol) and 4 mL of Et_2O at −78 °C was admitted CO (60 Torr, 0.297 mmol) from a calibrated gas bulb (91.0 mL). The solution was stirred for 20 h at −78 °C to give a pale yellow slurry. The solid was collected by filtration and dried briefly *in vacuo*, providing 140 mg of pale yellow powder (55% yield) that was stored at −20 °C.

c. CO Uptake from 11. A flask containing **11** (150 mg, 0.122 mmol) and 5 mL of hexanes at −78 °C was exposed to CO (344 Torr, 0.366 mmol) from a calibrated gas bulb. After stirring for 12 h at −78 °C, the

solution was degassed with the Toepler pump and the gas collected (0.145 mmol), indicating an uptake of 1.81 equiv of CO (0.221 mmol) per dimer. The solvent was removed and a ^{1}H NMR spectrum of the solid showed **20** (~95%) and **19** (~5%). Upon correction for the presence of **19**, the conversion required 1.85 equiv of CO per mol of **11**.

d. CO Uptake from 19. A flask containing **19** (200 mg, 0.163 mmol) and 6–7 mL of pentane at –78 °C was exposed to CO (449 Torr, 0.489 mmol) from a calibrated gas bulb. After stirring for 7 h at –78 °C, the solution was degassed with the Toepler pump and the gas collected (0.365 mmol), indicating an uptake of 0.76 equiv of CO (0.124 mmol) per dimer. The solvent was removed and a ^{1}H NMR spectrum of the solid showed ~75% **20** and ~25% **19**. Upon correction for remaining **19**, the conversion required 1.0 equiv of CO per mol of **19**.

e. Hydrolysis and H_2 Measurement. To a flask containing **20** (62 mg, 0.048 mmol) and 5 mL of hexanes at 77 K was added H_2O (0.563 mmol) from a calibrated gas bulb. After stirring for 1.5 h at 25 °C, the solution was degassed using the Toepler pump. The gas was passed through three liquid nitrogen traps, collected (0.046 mmol), and totally converted to H_2O upon circulation over CuO (300 °C), indicating that 0.96 equiv of H_2 evolved per **20**.

f. CH_3OH Measurement. Into a flask containing 125 mg of **20** (0.097 mmol) was distilled 1 mL of THF. An excess of H_2O(g) was admitted from a vacuum manifold (~8 equiv) to the flask at 77 K. Gas was evolved as the solution was warmed to 25 °C for 10 min. The solution was freeze–pump–thaw degassed, and acetone (72 Torr, 0.196 mmol) was admitted from a calibrated gas bulb as an internal standard. The flask was stoppered with a septum cap, and the solution was maintained at 0 °C during GC analysis. 2.00 equiv (0.194 mmol) of MeOH per **20** was found (acetone reference).

g. D_2O Quench. All glassware, including the portion of the vacuum line used in the D_2O transfer, was either rinsed or exposed to D_2O four times. To an NMR tube sealed to a 14/20 joint and attached to a 180° needle valve were added 60 mg of **20** (0.046 mmol) and 0.5 mL of C_6D_6. An excess of D_2O(g) (~0.5 mmol) was condensed in via the vacuum manifold at 77 K, and the tube was sealed with a torch. Vigorous bubbling ensued upon warming to 25 °C, and a ^{13}C NMR spectrum revealed a ~1:1 ratio of CH_2DOD and CHD_2OD.

19. [(silox)$_2$Ta]$_2$(μ-O)$_2$(μ-CHMe) (21). a. Synthesis. A flask equipped with a reflux condenser was charged with **20** (1.240 g, 0.966 mmol). Hexanes (15 mL) were added, and the solution was heated to 60 °C under Ar for 1 h. The resulting orange solution was filtered and concentrated to 2.5 mL. Upon cooling to –78 °C, the solution turned yellow and precipitated a white powder, which was collected by filtration and dried, yielding 754 mg of product (61% yield). Anal. Calcd for $Ta_2Si_4O_6C_{50}H_{112}$: C, 46.78; H, 8.79. Found: C, 46.57; H, 8.65. M_r found 1057, calcd 1284.

b. Hydrolysis. To a flask containing **21** (200 mg, 0.156 mmol) and 5 mL of toluene at –78 °C was added H_2O(g) (0.563 mmol) from a gas bulb. A white solid was generated as the solution stirred for 1.5 h at 25 °C. The solution was degassed using the Toepler pump, and the gas was passed through three dry ice/acetone traps, collected (0.151 mmol, 0.97 equiv), and identified as ethane by IR.

20. [(silox)$_2$Ta]$_2$(μ:η^1,η^1-CH=CHO)(μ:η^1,η^2-CH_2O)(μ-O) (22). a. Synthesis from 11. A flask containing **11** (860 mg, 0.700 mmol) and 30 mL of hexanes was cooled to –78 °C and exposed to 1 atm of CO. While the mixture stirred at –78 °C for 3 h, the orange color discharged to give a pale yellow slurry. The mixture was warmed to 25 °C and stirred for 10 h until a clear yellow solution resulted. Hexanes were removed *in vacuo* and the residue was filtered in Et_2O. Concentration of the solution to 3 mL, cooling to –78 °C, and filtration yielded 460 mg of white powder (50% yield). IR (Nujol): ν($^{12}C^{12}C/^{13}C^{13}C$) 1509/1458, ν($^{12}CO/^{13}CO$) 1218/1191 cm^{-1}. Anal. Calcd for $Ta_2Si_4O_6C_{48}H_{110}$: C, 46.70; H, 8.61. Found: C, 46.78; H, 8.47.

b. Synthesis from 20. An NMR tube sealed to a 14/20 joint was charged with **20** (12 mg, 0.009 mmol) and attached to a needle valve adapter. C_6D_6 (0.5 mL) was distilled into the tube, and then 180 Torr of CO (~0.08 mmol) was admitted at 77 K and the tube flame-sealed. After 1 h at 25 °C, NMR analysis showed a 95% yield of **22**.

c. CO Uptake. A flask charged with **11** (491 mg, 0.400 mmol) and 20 mL of hexanes was freeze–pump–thaw degassed three times, cooled to –78 °C, and exposed to CO (503 Torr, 2.49 mmol) from a calibrated gas bulb. After the mixture was stirred for 2 days at 25 °C, a clear yellow solution resulted, which was degassed with the Toepler pump. The residual gas was collected in a 192-mL volume (139 Torr, 1.45 mmol) and converted to CO_2 upon circulation over CuO (300 °C), indicating an uptake of 2.60 equiv of CO (1.04 mmol) per dimer. The yellow solid contained 90% **22** by ^{1}H NMR.

d. Hydrolysis. A flask charged with **22** (154 mg, 0.117 mmol) and 1.5 mL of THF was freeze–pump–thaw degassed three times and cooled to 77 K. Benzene was added as an internal standard via a calibrated gas bulb (0.112 mmol). An excess of H_2O (four 600-mL, 10-Torr portions; 1.3 mmol) was condensed into the flask at 77 K, and the solution was warmed to 25 °C and stirred for 0.5–2.5 h. Volatile materials from the resulting yellow solution were vacuum-transferred to a flask, from which samples were drawn for GC analysis (DBWax column). For NMR analysis, the molecule was similarly hydrolyzed by H_2O in THF-d_8, and the resulting volatiles were transferred *in vacuo* into an NMR tube. The tube was flame-sealed and warmed to 25 °C. Both methods showed acetaldehyde and methanol in a 1:1 ratio (0.5–0.7 equiv vs internal standard, depending upon the experiment).

21. [(silox)$_2$Ta]$_2$(μ:η^1,η^2-CH_2O)(μ-O_2) (23). a. Synthesis. A flask containing **13** (275 mg, 0.219 mmol) in 5 mL of hexanes was freeze–pump–thaw degassed three times and then exposed to CO (232 Torr, 0.655 mmol) from a calibrated gas bulb (52.0 mL). The solution was stirred for 12 h at 25 °C and then degassed with the Toepler pump. A total of 90 Torr of CO (0.407 mmol) was collected in a 83.3-mL volume and then converted quantitatively to CO_2 by cycling over CuO (300 °C), indicating an uptake of 1.13 equiv of CO per dimer (0.248 mmol). NMR analysis indicated an 82% yield of **23** as a white solid.

b. Hydrolysis. A total of 250 mg (0.195 mmol) of **23** from above was dissolved in 1 mL of THF-d_8. Benzene standard (50 Torr, 0.141 mmol) was admitted to the flask at 77 K from a calibrated gas bulb (52.0 mL), followed by an excess of H_2O (five 800-mL, 10-Torr portions; 2.2 mmol). The solution was warmed to 25 °C and stirred for 4 h, forming a yellow slurry. The volatile products were vacuum-transferred into an NMR tube, and methanol (0.131 mmol, 0.67 equiv) and a trace of (silox)H were identified as the only organic products.

22. [(silox)$_2$TaH](μ-O)$_2$[TaCH$_3$(silox)$_2$] (24). a. Synthesis. A flask containing **14** (230 mg, 0.185 mmol) and 5 mL of benzene was exposed to CO (131 Torr, 0.370 mmol) from a calibrated gas bulb (52.0 mL). The colorless solution was stirred for 18 h at 25 °C and then degassed with the Toepler pump. The gas was passed through three 77 K traps and then collected in a 21.7-mL volume (173 Torr, 0.204 mmol), indicating an uptake of 0.90 equiv of CO (0.166 mmol) per dimer. The solid residue contained >95% **24** by ^{1}H NMR. IR (Nujol): ν(TaH) 1804 cm^{-1}. FAB-MS (Nujol): *m/e* 1270 (21.2), 1271 (14.7), 1272 (18.8), 1273 (10.7).

b. Hydrolysis. To a freeze–pump–thaw degassed solution of **24** (225 mg, 0.177 mmol) in 5 mL of benzene was admitted an excess of H_2O vapor (five 800-mL, 10-Torr portions; 2.2 mmol) at 77 K. Gas evolution occurred as the mixture was warmed to 25 °C and stirred for 2 h. The resulting volatiles were passed through three –78 °C traps and collected via a Toepler pump in an 83-mL volume (73 Torr, 0.330 mmol). The H_2 was converted to H_2O by circulation over CuO (300 °C) and condensed into a –78 °C trap. The remaining gas was recollected in a 21.7-mL volume (151 Torr, 0.178 mmol, 1.01 equiv) and identified as CH_4 by ^{1}H NMR. By difference, 0.152 mmol (0.86 equiv) of H_2 was generated.

23. [(silox)$_2$Ta]$_2$(μ:η^2,η^1-OCHCH$_3$)(μ-O)$_2$ (25). An NMR tube sealed to a 14/20 joint was charged with 30 mg of **24** (0.02 mmol) and 0.5 mL of C_6D_6. The tube was attached to a needle valve adapter, and the solution was freeze–pump–thaw degassed three times. The evacuated tube was cooled to 77 K, an excess of CO (150 Torr) was admitted, and the tube was flame-sealed. After 6 days at 25 °C, >90% conversion was observed. Hydrolysis of **25** by the method described for **22**, above, yielded ethanol by ^{1}H NMR analysis.

Physical Studies. 1. 11 + H_2 Exchange by Magnetization Transfer. **11** (25 mg, 0.0204 mmol) was dissolved in 0.4 mL of toluene-d_8, and the solution was transferred to a sapphire NMR tube fitted with a titanium alloy valve, which was then pressurized with either 14.3 or 55.1 atm of H_2. T_1 measurements were made using a standard inversion recovery pulse sequence (T1IRCA) with a compensated 180° inversion pulse; the recycle delay for subsequent experiments was set to $5T_1$. Magnetization transfer spectra were initiated with a 9.5-ms inversion pulse obtained from the low-power transmitter with 30 dB attenuation and with the spectrometer frequency placed on either the free H_2 or the TaH resonance. Both the experimental technique and the analysis have been described previously.[51,62]

2. Isotope Scrambling in 11/11-d_4. A 5-mm base-washed NMR tube, sealed to a 14/20 joint, was charged with a 1:1 mixture of solid **11** and **11**-d_4 (5–40 mg) and attached to a needle valve adapter. With the evacuated tube cooled to 77 K, 0.75 mL of toluene-d_8 was added and the

tube was sealed under dynamic vacuum. The sample was kept at 77 K until immediately before it was mixed and inserted into the preshimmed 10 °C NMR probe for monitoring. The silox peak was typically suppressed by presaturation (5-s irradiation) in order to reduce the dynamic range of the spectrum and enhance observation of the hydride signals. First-order rate constants for the decay of **11** were calculated using a nonlinear least-squares fit to the approach-to-equilibrium equation: $[\mathbf{11}] = 0.125 + 0.875\exp(-kt)$, where $[\mathbf{11}]_0$ is standardized to 1.

3. Single-Crystal X-ray Diffraction Analysis of $[(silox)_2TaH_2]_2$ (11). An orange single crystal of $[(silox)_2TaH_2]_2$ (**10**), obtained from toluene solution, with dimensions 0.3 × 0.3 × 0.3 mm, was sealed in a Lindemann capillary. Preliminary X-ray diffraction photographs and analysis of preliminary data indicated a body-centered cubic lattice with $a = 28.125(6)$ Å as determined from a least-squares fit of 15 diffractometer-measured 2θ values at 25 °C. The space group was uniquely determined to be $I\bar{4}3d$, according to the systematic absences: hkl, $h+k+l = 2n$; hhl, $2h+l = 4n$. The cell volume was 22 247 Å^3 with a calculated density of 1.10 g/cm^3, where $Z = 12$ and $T = 25$ °C. All unique diffraction maxima with $2\theta \leq 40°$ were measured on a four-circle automated diffractometer with θ–2θ scans at 3 deg/min in θ using graphite-monochromated Mo Kα radiation ($\lambda = 0.710\,69$ Å). After correction for Lorentz polarization and background effects, 550 (46.2%) of the unique data (1190) were judged observed ($|F_o| \geq 3\sigma|F_o|$).[85] The structural solution proceeded using heavy atom methods. The asymmetric unit consists of $TaSiOC_{12}H_{28}$ with the tantalum atom on a crystallographic 2-fold axis (Wyckoff d). The tantalum atom position was determined from a Patterson synthesis and the Si and O atoms by Fourier recycling. The carbon atoms were located from successive difference electron density maps. Each $[(silox)_2TaH_2]_2$ molecule has crystallographic $\bar{4}$ symmetry with the molecular center at Wyckoff position a. Block diagonal least-squares refinement with the Ta, Si, and O atoms anisotropic, the carbon atoms isotropic, and hydrogen atoms fixed at ideal positions converged to residuals $R = 0.079$ and $R_w = 0.050$ ($w^{-1} = \sigma^2(|F_o|)$).[86] The paucity of data prevented meaningful anisotropic refinement of the carbon atoms, and no absorption correction was attempted ($\mu = 30.1$ cm^{-1}).

(85) Cromer, D. T.; Mann, J. B. *Acta Crystallogr., Sect. A* **1968**, *A24*, 321–324.

Acknowledgment. Primary support from the National Science Foundation and the Air Force Office of Sponsored Research is gratefully acknowledged, as are contributions from the Alfred P. Sloan Foundation, the Union Carbide Innovative Research Program, and Cornell University. We are obliged to Prof. Melvyn R. Churchill of SUNY, Buffalo, for X-ray data collection on $[(silox)_2TaH_2]_2$ (**11**). We also thank the Spencer T. and Ann W. Olin Foundation and the NSF for fellowship support (R.L.M.) and the NIH and NSF Instrumentation Programs for funding of the Cornell NMR Facility.

Supplementary Material Available: Variable-temperature NMR ($^{29}Si\{^1H\}$ and ^1H) spectra of **14a,b** and information pertaining to the X-ray structural investigation of $[(silox)_2TaH_2]_2$ (**11**) and tables summarizing crystal data, including data collection and solution/refinement, atomic coordinates, hydrogen atom coordinates, isotropic and anisotropic temperature factors, bond lengths, and bond angles (10 pages); table of observed and calculated structure factors (3 pages). Ordering information is given on any current masthead page.

(86) $R = \sum||F_o| - |F_c||/(\sum|Fo|)$; $R_w = \{\sum w(|Fo| - |F_c|)^2/\sum w(|F_o|)^2\}^{1/2}$.